THESIS FOR THE DEGREE OF DOCTOR OF PHILOSOPHY

Detection of Lipids and Proteins on Biological Surfaces using Imaging Mass Spectrometry

LOUISE CARLRED

Department of Physics

CHALMERS UNIVERSITY OF TECHNOLOGY

Göteborg, Sweden 2016

Detection of Lipids and Proteins on Biological Surfaces using Imaging Mass Spectrometry

Chemistry, Materials and Surfaces
SP Technical Research Institute of Sweden
SE-501 15 Borås
Sweden
Telephone + 46 (0)10-516 5242

Department of Physics
Chalmers University of Technology
SE-412 96 Gothenburg
Sweden
Telephone + 46 (0)31-772 1000

Front page: Schematic illustrations of the different liposome approaches used in the thesis for simultaneous detection of lipids and proteins in tissue sections for detection of Amyloid-β peptides (red), sulfatides (green) and cholesterol (blue), or for multiplexed detection of the vitamin biotin (green) and the glycosphingolipid GM1 (red) in a supported lipid bilayer. For more details, see Fig. 13, 17 and 21 in the thesis.

Detection of Lipids and Proteins on Biological Surfaces using Imaging Mass Spectrometry

Louise Carlred
Department of Physics
CHALMERS UNIVERSITY OF TECHNOLOGY

ABSTRACT

Time-of-flight secondary ion mass spectrometry (ToF-SIMS) is a technique that can be used for imaging the spatial distribution of many different molecules at the same time. It is very sensitive for detection of small biomolecules, such as lipids, whereas larger biomolecules, such as peptides and proteins, cannot be detected as intact entities due to fragmentation. In this work, we have explored an alternative approach for detection of peptides and proteins with ToF-SIMS, using liposomes for labeling the target of interest. In this way, both lipids and proteins can be imaged at the same time, which opens up for the opportunity to investigate lipid-protein interactions.

The method has been applied for detection of biomolecules on two different biological surfaces; (1) a model surface containing controlled concentrations of target biomolecules bound to the substrate and (2) brain tissue sections from Alzheimer's disease transgenic mice. Other techniques, such as fluorescence microscopy and quartz crystal microbalance with dissipation monitoring (QCM-D), have also been used for the characterization of liposomes binding to the surface. Another imaging mass spectrometry technique, matrix-assisted laser desorption/ionization (MALDI), was also employed on mouse brain tissue sections for detection and investigation of amyloid-β deposits, a peptide associated with Alzheimer's disease.

This thesis thus shows how different techniques can be combined for investigation of biomolecules on complex biological surfaces, in order to potentially provide new information about the mechanism of neurodegeneration in Alzheimer's disease.

Keywords: Imaging Mass Spectrometry, ToF-SIMS, MALDI, QCM-D, Alzheimer's disease, Amyloid-β, phospholipids, cholesterol, sulfatides, GM1

APPENDED PAPERS

I. "Liposome binding for multiplexed biomolecule detection and imaging using ToF-SIMS" Sjövall, P., Agnarsson, B., <u>Carlred, L.</u>, Gunnarsson, A. and Höök, F. (2014) Surface and Interface Analysis, 46(10-11), 707-711.

II. "Simultaneous Imaging of Amyloid-β and Lipids in Brain Tissue using Antibody-Coupled Liposomes and Time-of-Flight Secondary Ion Mass Spectrometry" <u>Carlred, L.</u>, Gunnarsson, A., Solé-Domènech, S., Johansson, B., Vukojević, V., Terenius, L., Codita, A., Winblad, B., Schalling, M., Höök, F., Sjövall, P. (2014) J. Am. Chem. Soc.,136 (28), pp 9973–99.

III. "Imaging of Amyloid-β in Alzheimer's disease transgenic mouse brains with Time-of-Flight Secondary Ion Mass Spectrometry using Immunoliposomes" <u>L. Carlred</u>, V. Vukojević, B. Johansson, M. Schalling, F. Höök, P. Sjövall. (2016) Biointerphases, 11, 02A312.

IV. "Probing Cerebral Amyloid-β Pathology in transgenic Alzheimer's disease (ARCSWE) mice using MALDI Imaging Mass Spectrometry" <u>L. Carlred</u>, W. Michno, P. Sjövall, S. Syvänen, J. Hanrieder. (2016) Journal of Neurochemistry, (Accepted Article), doi: 10.1111/jnc.13645.

V. "Liposome Approach for Multiplexed Quantification of Biomolecules at Surfaces using Time-of-Flight Secondary Ion Mass Spectrometry" <u>L. Carlred</u>, B. Agnarsson, F. Höök and Peter Sjövall (in manuscript).

CONTRIBUTION REPORT

PAPER I: *I took part in the experimental work of the study, including liposome preparation and characterization, and the QCM-D analysis. I took part in the preparation of the paper.*

PAPER II: *I designed, optimized and performed the experimental work of the study. I wrote the main part of the paper.*

PAPER III: *I designed, optimized and performed the experimental work of the study. I wrote the main part of the paper.*

PAPER IV: *I took part in designing, optimizing and performing the MALDI experimental work of the study together with J.H. W.M. performed the immunohistochemistry and the laser microdissection experiments and J.H. was responsible for the statistical analysis. I wrote the main part of the paper together with J.H.*

PAPER V: *I took part in designing, optimizing and performing most of the experimental work of the study, including liposome preparation, QCM-D and ToF-SIMS analysis. B.A. was responsible for the fluorescence microscopy analysis. I wrote the main part of the paper together with P.S.*

CONTENTS

LIST OF ABBREVIATIONS

Aβ – Amyloid-β

AD – Alzheimer's disease

AF – Ammonium formate

ApoE – Apolipoprotein E

APP – Amyloid-β precursor protein

CHCA – α-cyano-4-hydroxycinnamic acid

DAPI – 4',6-diamidino-2-phenylindole

DHA – Docosahexaenoic acid

DHB – 2,5-dihydroxybenxoic acid

CSF – Cerebrospinal fluid

FD – Freeze-drying

IHC – Immunohistochemistry

IMS – Imaging mass spectrometry

MALDI – Matrix-assisted laser desorption/ionization

MCI – Mild cognitive impairment

MIF – Macrophage migration inhibitory factor

MRI – Magnetic resonance imaging

NFT – Neurofibrillary tangles

NaAc – Sodium Acetate

PET – Positron emission tomography

PBS – Phosphate buffered saline

PC – Phosphatidylcholine

PFA – Paraformaldehyde

PF – Plunge-freezing

PS1/2 – Presenilin 1/2

RT – Room temperature

SA – Sinapinic acid (3,5-dimethoxy-4-hydroxycinnamic acid)

SEM – Scanning electron microscopy

TFA – Trifluoroacetic acid

ToF-SIMS – Time-of-flight secondary ion mass spectrometry

QCM-D – Quartz crystal microbalance with dissipation monitoring

1. INTRODUCTION

The plasma membrane constitutes the protective barrier that surrounds all cells in the human body (Alberts 2002; Siegel and Ebrary 2006). The major components of the plasma membrane are lipids, which due to their hydrophobic and hydrophilic regions form a self-assembled bilayer that provides an efficient shield against the surrounding aqueous environment. In addition to their structural and protective function in the plasma membrane, lipids are highly involved in other processes in the cell, such as regulating intracellular trafficking (Lippincott-Schwartz and Phair 2010) and participating in cellular signaling, which controls cell growth, migration and death (Wenk 2005).

Other important components in the cell membrane are membrane proteins (Alberts 2002). The membrane proteins are involved in a variety of cellular functions, such as communication of the cell with the environment, participation in catalytic processes, and transportation of substances in or out of the cell. Activation of a membrane protein, usually through ligand binding, can result in a signaling cascade within the cell, which is also why the majority of all drugs today target the membrane proteins (Arinaminpathy 2009).

However, it is often not the lipids or proteins *per se* that are responsible for the signaling events in the cell. Recent research has shown that interactions between lipids and proteins in the cell membrane highly affects the signaling activity, for example by creating specific microenvironments in the lipid bilayer called lipid rafts (Simons and Toomre 2000). These rafts have different properties depending on their lipid and protein content, and also depending on other proteins or ligands attached to the raft-associated protein (Sheets et al. 1999). Most lipid rafts consist mainly of sphingolipids and cholesterol, and tend to form distinct liquid-ordered phases within the lipid bilayer due to the long and saturated fatty acid chains of the sphingolipids in combination with the hydrophobicity and rigidity of cholesterol. Cholesterol, in particular, has been found to influence the existence and activity of lipid rafts (Pralle et al. 2000).

Dysregulation of lipids in the cell can result in the generation of various diseases, for example by disrupting or promoting particular processes in the plasma membrane, many of which depend on lipid-protein interactions. One example is Alzheimer's disease (AD), for which it has been suggested that association of different lipid rafts in the plasma membrane is important for the formation of amyloid-β (Aβ) peptides, whose aggregation into so called

senile plaques is considered to be one of the main hallmarks of AD (Ehehalt 2003). In particular, it has been found that cholesterol is involved in the Aβ aggregation process (Di Paolo and Kim 2011; Puglielli et al. 2003). However, it is not known exactly how these processes occur or why the balance is disrupted. It is therefore important to study these interactions more thoroughly. Many different methods exist that can be used to study proteins or lipids separately, however, very few can study these molecules at the same time, which is vital for investigation of the interactions between lipids and proteins.

The aim of this thesis was to develop a new method for simultaneous imaging of both lipids and proteins by combining methods traditionally used in immunohistochemistry (IHC) with imaging mass spectrometry (IMS). The method has been applied to detect Aβ deposits and surrounding distributions of several lipids in transgenic AD mouse brains using time-of-flight secondary ion mass spectrometry (ToF-SIMS). Furthermore, the potential for simultaneous detection of many different biomolecules, so called multiplexing, was demonstrated on model surfaces, by quantitative detection of two different targets, namely the vitamin biotin and the glycosphingolipid GM1. The mouse brains were also investigated with matrix-assisted laser desorption/ionization (MALDI), for more thorough characterization of the Aβ deposits. Together, this work demonstrates the compatibility and complementarity of different methods for investigation of the complex biomolecular processes involved in AD.

2. BACKGROUND

2.1 ALZHEIMER'S DISEASE

AD is the most common form of dementia, which affects nearly 50 millions of people around the world (Ballard et al. 2011; M. Prince 2015). The most common symptoms of AD are loss of memory and cognitive function, resulting in decreased ability to handle simple tasks (St George-Hyslop 2000). The main reason for the development of AD is degeneration of nerve cells in the brain, especially in the hippocampus and cortex regions, which are the regions of learning and memory. But the reason for this neurodegeneration is not yet completely understood.

One of the main diagnostic features of AD is the accumulation of senile plaques between nerve cells in the brain, consisting of aggregates of the peptide Aβ. Another diagnostic hallmark of AD is the formation of neurofibrillary tangles (NFT) inside the nerve cells, consisting of aggregates of a protein called Tau. The formation of these plaques and tangles seems to be connected with the degeneration of nerve cells, but it is not clear how or why the aggregation of these molecules occur. Even though there is a clear connection between the extent of NFT and the severity of dementia (Arriagada et al. 1992), this pathology is not unique for AD, but a common feature for many types of dementia (Ballatore et al. 2007). In contrast, there is no clear correlation between the extent of Aβ plaques and the severity of the dementia (Terry et al. 1991), suggesting that there are more components involved in the neurodegenerative processes in AD. One hypothesis is that the generation of Aβ plaques is a less toxic and final product of the degenerative process, whereas the soluble oligomeric forms of Aβ peptides, which are precursors to the formation of the plaques, have the most toxic properties, by interfering with the synapses that connect the nerve cells during signal transduction (Gouras et al. 2015; Selkoe 2008; Walsh and Selkoe 2007). Furthermore, it has been found that these soluble, pre-fibrillar Aβ peptides accumulate inside the nerve cells, in endosomal vesicles and in the synaptic compartments, at early stages of AD, before extracellular Aβ deposition is detectable (Gouras et al. 2013).

The Aβ peptide is formed through two sequential cleavages of the Amyloid-β precursor protein (APP); the catalytic transmembrane proteins β-site APP cleavage enzyme 1 (BACE1), also referred to as β-secretase 1, which cleaves APP at the amino-terminal region of the Aβ sequence, followed by multiple actions of the γ-secretase complex, which consists of two

proteins derived from the *presenilin* (PS) 1 and 2 genes (LaFerla 2002; Siegel and Ebrary 2006). Genetic mutations on APP or PS1/2 are the most common causes of familial AD, which often results in early-onset AD (< 65 years). These mutations often result in either enhanced production of Aβ peptides, as in the case of the Swedish double mutation (APPswe) (Citron et al. 1992), or enhanced production of the specific version of Aβ with 42 amino acids (Aβ42), which is the longer and more aggregation-prone Aβ peptide, compared to the Aβ40 peptide. However, only about 5% of all incidences of AD have been found to be caused by genetic mutations (Ballard et al. 2011). Thus, the majority of AD incidences is referred to as the sporadic form of AD, and has usually a late-onset age (> 65 years).

The currently known main risk factor for sporadic AD is, besides from ageing, the possession of a specific allele, ε4, of a gene that codes for a protein called apolipoprotein E (ApoE) (Siegel and Ebrary 2006). ApoE is involved in the dynamic regulation of lipids, and in particular the transportation of cholesterol, in the brain. Cholesterol is an important component of the plasma membrane and the myelin sheath that surround the axons of the nerve cells. Recent research has shown that dysregulation of cholesterol is involved in the generation of different neurodegenerative diseases, including AD (Di Paolo and Kim 2011; Puglielli et al. 2003). Especially, the transportation of cholesterol into the cells seems to be closely connected to the formation of Aβ peptides, as well as the aggregation of Aβ into toxic oligomers and fibrils. Also, cholesterol has been found to regulate the activity of APP cleavage into Aβ, by merging β- and γ-secretases into APP containing lipid rafts that are present in the cell membrane (Ehehalt 2003). Furthermore, ApoE has been shown to directly bind to Aβ and promote the aggregation or clearance of Aβ, possibly in an isoform dose-dependent manner, where the ε4 allele seems to promote Aβ aggregation while the ε2 allele have a more protective function, by promoting clearance of Aβ (Kim et al. 2009).

Many other lipids have been found to be involved in the generation of Aβ and AD, such as ceramides, sphingomyelin and glycosphingolipids (Di Paolo and Kim 2011). In particular, the glycosphingolipid GM1 has been found to bind to Aβ and promote the aggregation into Aβ fibrils by acting as a seed, especially in combination with increased levels of cholesterol in the cell membrane (Kakio et al. 2001; Yanagisawa 2007). Other studies have shown that the ceramide levels are highly increased in brain tissue from subjects with mild cognitive impairment (MCI), an early stage of AD, at the same time as the sulfatide levels are depleted, which further indicates that dysregulation of lipids is an important factor in AD (Han 2010).

However, more research is needed to understand how these different components are connected.

Unfortunately, there are no treatments available today that can cure AD. Most prescribed drugs alleviate some of the symptoms at the early stages of the disease. One type of commonly prescribed drugs for this purpose is cholinesterase inhibitors, which prolong the signaling between cholinergic neurons by preventing the degradation of the neurotransmitter acetylcholine that is released into the synapse (St George-Hyslop 2000). Other commonly prescribed drugs are antipsychotics and antidepressants, which have been shown to have limited benefits (Ballard et al. 2011). However, many other treatments are under investigation and some of them have reached phase 3 in clinical trials. One approach that seems promising is immunotherapy, which involves the use of antibodies to target and promote clearance of Aβ in the brain. Earlier studies have shown that the injection of antibodies decreased Aβ deposition and improved cognitive behavior in transgenic mouse models (Thakker et al. 2009). However, clinical trials with AD patients have shown mixed results (Ballard et al. 2011).

Another interesting approach for targeting Aβ is to prevent the formation of new Aβ peptides, using β- or γ-secretase inhibitors. Several drugs for this purpose have reached phase 3 in clinical trials, although none have yet succeeded further. One problem with inhibiting the γ-secretases is that these enzymes also modulate the activity of other important proteins in the cell (Gouras et al. 2015). Other interesting therapies include intake of natural products such as Vitamin E, omega 3 fatty acids and in particular the fatty acid docosahexaenoic acid (DHA), which is under investigation in phase 3 clinical trials. Other potential drugs include modulation or stabilization of Tau aggregates, which have shown some promising results in early-phase clinical trials (Ballatore et al. 2007).

Another type of drugs extensively evaluated as potential candidates for the treatment or prevention of AD is the cholesterol-lowering drugs statins. Statins inhibit the endogenous production of cholesterol in the cells, and have been used for many years by people with elevated blood cholesterol levels, in order to prevent cardiovascular disease. Since the link between cholesterol dysregulation and AD was discovered, statins were suggested as a potential treatment. Many epidemiological and clinical studies have tried to evaluate the benefit of statins in AD prevalence and their effect on cognitive function, although with mixed results (Barone et al. 2014). Even though some of the epidemiological studies did show

a protective effect and reduced risk of developing AD, several randomized phase 3 clinical trials have shown no benefit of statins on cognitive function.

One of the reasons why many drugs fail, or appear ineffective, in the clinical trials might be that the disease progression has already gone too far when the symptoms start to appear. Improved diagnosis of AD and earlier treatment would therefore be of great benefit. In fact, there are no techniques today that can definitely diagnose AD, or distinguish it from other types of dementia, until post mortem analysis. Instead, a probable diagnosis is being made based on several different criteria, which are derived through neuropsychological assessment in combination with a neuropathological indication, such as apparent brain atrophy in specific brain regions, as revealed by structural magnetic resonance imaging (MRI) scans, or aberrations in levels of Aβ42 or Tau in the cerebrospinal fluid (CSF) (Ballard et al. 2011).

Another newly developed technique that can be used for AD diagnosis *in vivo* is positron emission tomography (PET). By using specific markers, such as ^{18}F-fluorodeoxyglucose, PET imaging can detect decreased glucose metabolism, which is an indication of AD. Furthermore, by using the ^{11}C-labeled Pittsburgh compound B, which binds to Aβ oligomers, it can reveal increased amyloid load in the brain. Recently, a study investigated the distribution of Tau pathology in the brain using PET imaging with a specific marker for Tau (^{18}F-AV-1451) (Schöll et al. 2016). The study was able to distinguish AD disease progression by visualizing the distribution of Tau in combination with increased amyloid burden in specific brain regions in AD patients, compared to non-demented elderly subjects. Further investigations of these promising techniques and the discovery of other AD-specific biomarkers, in the CSF (Zetterberg et al. 2010) and in the blood (Thambisetty and Lovestone 2010), increases the possibility to detect and treat AD before significant damage occurs in the brain.

Immunohistochemistry

A general method for investigating the pathological mechanisms of diseases is to image tissue sections with optical microscopy (Swedlow 2012). Often different kinds of stains are used as markers of specific cell features, such as cell nuclei or protein aggregates (Fig. 1A). This method was used already a century ago, when Dr. Alois Alzheimer first discovered the pathological hallmarks of AD by investigating brain tissue from a patient with severe dementia (Cipriani et al. 2011).

To be able to target and visualize a specific protein in tissue samples, immunohistochemistry (IHC) can be applied. In IHC, specific antibodies are used that recognize the molecule of interest. These antibodies can be directly conjugated with a fluorophore, for detection with fluorescence microscopy. However, in order to amplify the signal, a subsequent secondary antibody labeled with the fluorophore is often used (Fig. 1B). While the so called primary antibody usually recognizes a very specific part of the target molecule, called the epitope, the secondary antibodies are usually designed so that they recognize many different epitopes on the primary antibody, thereby enabling the binding of several secondary antibodies to each primary antibody, resulting in amplification of the fluorescence signal. In this way, very low concentrations of the target molecules can be localized in the sample. Furthermore, several different targets can be localized in the tissue at the same time using different antibodies labeled with fluorophores with spectrally distinct fluorescence properties (Jensen 2014).

However, IHC is limited to the availability of antibodies to the target of interest, and many antibodies today are hampered by specificity problems (O'Hurley et al. 2014). Also, the selection of secondary antibodies must be done carefully to avoid cross-reactivity and to avoid spectral overlap of the fluorophores for specific detection of each target (Lichtman and Conchello 2005). Therefore, only 3-4 different targets can normally be imaged at the same time when using standard microscopes, although, using a combination of a very sensitive imaging spectrometer with appropriate dyes, designed filter sets, and a signal isolation algorithm, up to seven different fluorophores have been detected at the same time in a tissue section (Tsurui et al. 2000). However, even if antibodies are good for targeting for example proteins, many other molecules, such as individual lipids, are lacking a specific epitope that can be targeted by an antibody, and can thus not be detected with this method. This, in turn, complicates co-localization analysis and investigation of possible interactions between lipids and proteins.
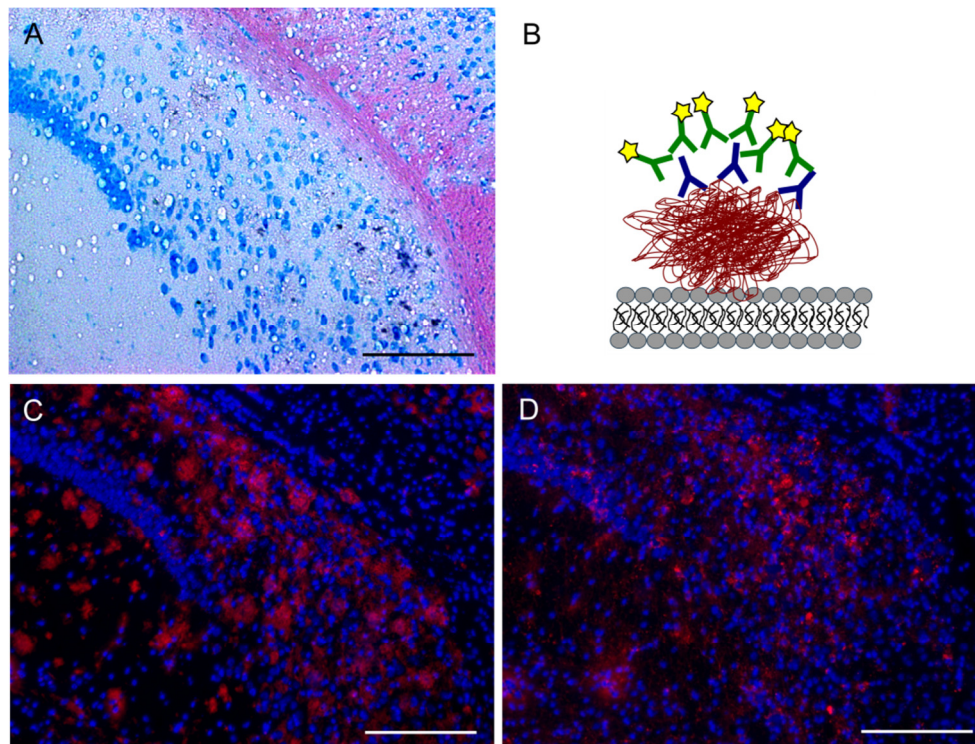
Figure 1 (A) Optical (bright field) image of the hippocampal region (CA1) of a transgenic AD mouse brain stained with eosin methylene blue, showing major tissue structures such as cell nuclei (blue) and the white matter of corpus callosum (red). (B) Schematic illustration of the principles of IHC by binding of primary antibodies (blue) to the protein of interest (red) followed by secondary antibodies (green) with fluorescent tags (yellow). (C-D) Fluorescence images of the hippocampal region (CA1) in two adjacent tissue sections from a transgenic AD mouse brain showing (C) Aβ plaques (red), stained with primary (6E10) + secondary (Alexa 555 goat anti-mouse) antibodies, and (D) NFT (red), stained with primary (AT8) + secondary (Alexa 555 goat anti-mouse) antibodies. Surrounding cell nuclei is counterstained with DAPI (blue). Scale bar = 200 µm.

Imaging mass spectrometry

Imaging mass spectrometry (IMS) is a methodology that can be used for imaging of both lipids and proteins in biological samples (Chughtai and Heeren 2010; Pol et al. 2010; Touboul et al. 2011). One of the most common IMS techniques is matrix-assisted laser desorption/ionization (MALDI), in which a laser is used to produce ions specific to the molecules at the surface of the sample. To prevent fragmentation of the analytes during the laser-induced desorption and to enhance the ionization probability, the tissue sample is prior to analysis sprayed with an organic compound, a so called matrix, which covers the surface of the sample. The ions produced by the laser are then separated by a mass analyzer and detected to produce a mass spectrum, in which the mass-to-charge ratios (*m/z*) of the individual peaks are used for identification of the detected ions and molecules. In this way, intact molecules up to ~100 kDa in mass can be identified and detected on the surface. One disadvantage of MALDI is that the matrix can interfere with the detection of small molecules that are in the same mass range as the matrix compounds (usually <500 Da, depending on the matrix),

thereby excluding the detection of small lipids such as cholesterol (m/z = 369-385). Also, different matrices are often needed for detection of different types of molecules, depending on the properties of the analytes (Chughtai and Heeren 2010). Simultaneous detection of lipids and proteins is therefore difficult to accomplish with this method, especially since detection of proteins usually requires additional rinsing steps to remove lipids and other interfering molecules from the surface before application of the matrix. Furthermore, the spatial resolution of MALDI imaging is limited to the spot size of the laser beam, which normally is ~50 µm, although, some studies have reported spatial resolutions in the 5-10 µm range, using a special instrumental setup (Römpp and Spengler 2013). Nevertheless, due to the soft ionization and dynamic molecular range, MALDI imaging has become a popular tool in the biomedical field for detection of peptides and proteins (Caprioli et al. 1997; Hanrieder et al. 2011; Rohner et al. 2005), as well as lipids (Benabdellah et al. 2010; Cerruti et al. 2012) and pharmaceuticals (Stoeckli et al. 2007) in tissue sections.

Another IMS technique that can be used for imaging of tissue samples is time-of-flight secondary ion mass spectrometry (ToF-SIMS); (Claudia Bich et al. 2015; Alain Brunelle and Laprévote 2009; Passarelli and Winograd 2011). In ToF-SIMS, a focused ion beam is pulsed upon the sample to produce secondary ions, which are emitted from the sample surface without the need for a matrix. The emitted secondary ions are collected and separated into a mass spectrum for identification of molecular species on the surface. Using this method, molecules can be detected and localized on the sample surface with a spatial resolution <1 µm. However, because of fragmentation of the molecules during sputtering, only ions up to ~2 kDa are typically created with this technique, limiting the detection to molecules with low mass, such as lipids, while larger molecules, such as proteins, become too fragmented to be detected as intact molecules. Nevertheless, due to the label-free detection of many other biomolecules with high spatial resolution, ToF-SIMS has been successfully used for imaging of biological samples, for example for investigation of the lipid distribution in mouse brains tissue (Nygren et al. 2005; Sjövall et al. 2004; Touboul et al. 2004), muscle tissue (Tahallah et al. 2008), adipose tissue (Belazi et al. 2009) and bone tissue (Henss et al. 2016). Lipid distributions have also been successfully mapped in individual cells, for example in *tetrahymena thermophila* during mating (Ostrowski et al. 2004), and in single neurons (Monroe et al. 2005). Other small compounds, such as pharmaceuticals, have also been investigated with ToF-SIMS, for example for determination of the distribution of specific drugs in skin tissue (Sjövall et al. 2014).

ToF-SIMS is usually conducted under so called static SIMS conditions, in which the data is obtained from a sample surface that has not yet been significantly damaged by the (pulsed) primary ion beam. An IMS technique similar to ToF-SIMS is dynamic SIMS, which uses a continuous primary ion beam and instead interrogates a sample surface that is under continuous alteration by the primary ion beam (Boxer et al. 2009). Advantages with dynamic SIMS are the high sensitivity and the high spatial resolution that can be obtained (<50 nm), for example, using the so called NanoSIMS instrument (Guerquin-Kern et al. 2005). However, the molecular structures on the sample surface are normally lost during the ion bombardment, resulting in the production of mostly monatomic or diatomic secondary ions. Therefore, isotopic labels are typically used to obtain molecular information from the sample surface, for example through incorporation of metabolic stable isotope-labeled lipids in cultured cells (Frisz et al. 2013; Yeager et al. 2016). To be able to detect proteins with NanoSIMS, functionalized antibodies tagged with different isotopic metal reporters have been used, enabling the detection of ten different targets at the same time in a tissue sample from human breast tumors (Angelo et al. 2014). Lipids, however, remained unseen with this approach. A similar approach for detection of a specific protein in cells has also been used, by targeting the protein with antibodies tagged with fluorinated gold colloids, while at the same time detecting lipids labeled by incorporated metabolic isotopes (Wilson et al. 2012). Others have previously also used isotope-labeled metabolites to detect specific biomolecules with NanoSIMS (Steinhauser and Lechene 2013). This method, called multi-isotope imaging mass spectrometry (MIMS), has revealed both protein distributions (using isotope-labeled amino acids) (Zhang et al. 2012), and DNA synthesis (using isotope-labeled thymidine) (Steinhauser et al. 2012) at subcellular resolution.

Combining IMS with microscopy

Instead of using only one of the mentioned imaging techniques above, it is also possible to combine the imaging techniques for subsequent detection of different biomolecules. In a study by Solé-Domènech et al., the distributions of cholesterol and sulfatides were studied in brain tissue from an AD transgenic mouse model and correlated to Aβ deposits using confocal laser scanning fluorescence microscopy (Solé-Domènech et al. 2013). To avoid redistribution of lipids during the tissue preparation, the Aβ deposits were first stained in an adjacent tissue section, for localization of regions of interest. The untreated other half of the tissue section was then analyzed with ToF-SIMS in the identified regions of interest for localization of lipids, and then subsequently stained for various biomarkers and imaged with fluorescence microscopy to confirm that matching regions were indeed examined. In this way, Aβ deposits could be correlated with the cholesterol distribution in the tissue, together with activated microglia and astrocytic processes (Fig. 2). A similar study also investigated the distribution of cholesterol in cortical brain tissue from AD patients and tried to correlate the amount of cholesterol with subsequent staining of Aβ and Tau (Lazar et al. 2013). Although no clear correlation was found between the increased cholesterol distribution and the deposits, it was found that AD patients had significantly higher amounts of cholesterol in the cortex compared to control samples.

Another study has investigated the feasibility of imaging the same tissue section with optical microscopy and ToF-SIMS, by investigating the lipid distribution before and after histological staining (C. Bich et al. 2013a). Here, it was found that when excluding the fixation and dehydration steps from the staining protocol, it was still possible to image the tissue section with ToF-SIMS for localization of cholesterol in major anatomical regions, although, some distention of the tissue was observed when comparing the stained tissue section with a reference sample. A similar study investigating the feasibility of MALDI imaging on stained tissue sections has shown that some stains can interfere with the ionization process, by suppressing certain molecules in the mass spectrum (Chaurand et al. 2004). However, by staining the tissue section after MALDI imaging, it was possible to correlate major histological features with several different protein markers detected in the MALDI mass spectrum (Deutskens et al. 2011). These studies further strengthen the need for complementary analyses with different techniques for detection of a broader range of molecules in the same tissue section.
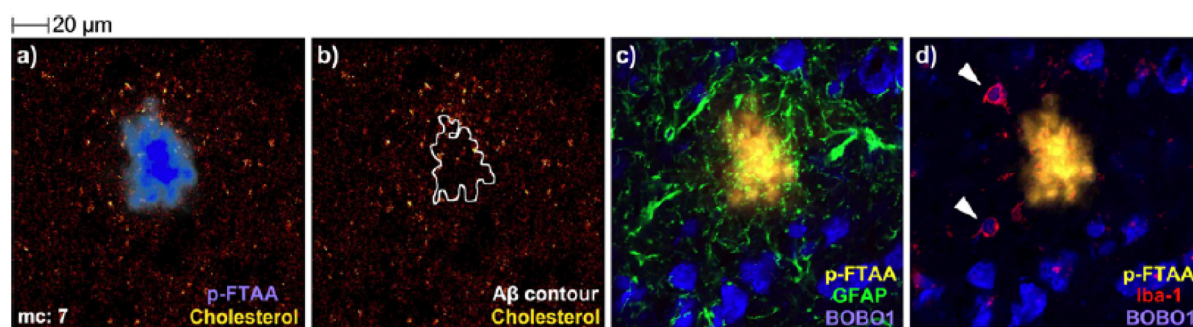
Figure 2 (a-b) Colocalization of the cholesterol distribution (yellow) and Aβ deposits (p-FTAA, blue) in AD mouse brain tissue using ToF-SIMS imaging and confocal fluorescence microscopy, respectively. (c-d) Detection of activated astrocytic processes (GFAP, green) and reactive microglia (Iba1, red, indicated with arrows) in the vicinity of the same Aβ deposit as in (a), stained with p-FTAA (yellow). Surrounding cell nuclei are stained with BOBO-1 (blue). mc = maximum counts in one pixel. Reprinted with permission from (Solé-Domènech et al. 2013). Copyright 2012, Springer-Verlag.

2.3 LIPOSOMES FOR DETECTION OF BIOMOLECULES ON SURFACES

A liposome is a water containing vesicle surrounded by a lipid membrane, called a lipid bilayer (Fig. 3A) (Alberts 2002). The formation of liposomes is highly dependent on the nature of the lipid molecules, and different lipids are prone to form different forms of assemblies. The most common type of lipids forming lipid bilayers is phospholipids. Phospholipids consist of a polar head group and two hydrophobic fatty acid tails, which, in general, give the molecule a cylindrical shape. The different parts of the phospholipid also give the molecule its amphiphilic properties, where the polar head group favors an aqueous environment and the tails prefer a hydrophobic environment. This is why phospholipids tend to spontaneously form lipid assemblies in an aqueous solution, since these structures are energetically favorable by providing the head group to be in contact with the surrounding water while the tails are closely packed within the assembly. It is because of the cylindrical shape of the phospholipids that these lipids are prone to form lipid bilayers and liposomes, since in this assembly the molecules become closely packed and thereby protected from the environment. However, depending on the size of the head group and the tails, some phospholipids can also form a more cone-like structure, which are more prone to accumulate in curved membranes (Ostrowski et al. 2004).

Since phospholipids form lipid bilayer assemblies spontaneously in an aqueous solution, liposomes can easily be produced artificially, usually through drying of a dissolved lipid mixture on a surface, followed by hydration in a desired buffer and sonication and/or membrane extrusion, to produce homogeneous and unilamellar liposomes of a particular size (Jousma et al. 1987; Patil and Jadhav 2014). In this way, liposomes with different lipid compositions can be produced. The included lipids can also be labeled with different tags,

such as fluorophores or ligands, thereby functionalizing the liposomes in different ways (Gunnarsson et al. 2010a). By including fluorescently labeled lipids, the liposomes can be detected and studied with fluorescence microscopy. One ligand often used to functionalize biomolecules is the vitamin biotin, which is a small molecule that binds to the proteins avidin, streptavidin and the bioengineered variant neutravidin (Nilebäck et al. 2011). Since these proteins contain four binding sites for biotin, they can bind to different biotinylated molecules simultaneously, thereby linking the biomolecule with other molecules containing a biotin-tag, such as an antibody (Fig. 3B). In this way, specific proteins of interest can be labeled with biotinylated liposomes, for subsequent detection with fluorescence microscopy, or with ToF-SIMS, using specific deuterated lipids to distinguish the liposomes from the native lipids in the tissue (Gunnarsson et al. 2010a).

The antibody can then be changed depending on the target of interest, and by varying the lipid composition in the liposomes this approach can also be used for detection of multiple targets at the same time. However, in this case the antibodies need to be directly conjugated to each liposome, for unique identification. This can be achieved by including a lipid with a reactive group, such as a maleimide, in the liposomes, and introducing thiol groups on the antibodies, since thiols react spontaneously with maleimides to form a stable chemical bond (Jølck et al. 2010; Nobs et al. 2004). These antibody-conjugated liposomes, so called immunoliposomes, have been used previously as drug delivery vehicles, for targeted delivery of drugs to specific sites of the body (Allen and Cullis 2013; Huwyler et al. 1996; Park et al. 1995). In this work, we show that the immunoliposomes, and other protein-conjugated liposomes, can be used for biosensing purposes, for multiplexed detection of molecules at biological surfaces (Fig. 3C).

Figure 3 Schematic illustrations of (A) a liposome as a vesicle surrounded by a lipid bilayer, (B) the liposome-based approach for detection of the protein of interest (red) by using biotinylated antibodies (dark blue) followed by the biotin-binding protein neutravidin (green) and biotinylated liposomes (light blue) with fluorescent tags (yellow), and (C) antibody-conjugated liposomes (immunoliposomes) for detection of multiple targets on the surface.

3. EXPERIMENTAL METHODS

The main methods used in this thesis were quartz crystal microbalance with dissipation monitoring (QCM-D), fluorescence microscopy, time-of-flight secondary ion mass spectrometry (ToF-SIMS) and matrix-assisted laser desorption/ionization (MALDI). QCM-D was used to investigate and verify specific binding of the liposomes to targets on model surfaces. Fluorescence microscopy was used to verify specific binding of antibodies to Aβ in tissue sections, either using fluorescent secondary antibodies or with liposomes containing the fluorescent markers, as well as for detection of liposome binding to model surfaces. ToF-SIMS was the central and most critical experimental method used, as it provided the parallel imaging of native lipids and liposomes bound to Aβ deposits in tissue sections, but also multiplexed target detection on model surfaces. Furthermore, MALDI imaging was used as a complementary method to gain deeper knowledge about the Aβ deposit composition and other proteins in the microenvironment.

3.1 LIPOSOME PREPARATION AND CONJUGATION WITH ANTIBODIES

The liposomes were prepared according to the film method (Jousma et al. 1987), by mixing the desired composition of lipids, dissolved in methanol/chloroform, in a round bottom flask followed by drying, first in a flow of nitrogen gas and then at reduced pressure using a vacuum pump for 1 hour. The dried lipid film was then hydrated in the desired buffer, which was phosphate buffered saline (PBS, pH 7.4) for the biotinylated liposomes and sodium acetate (NaAc, pH 5) for the immunoliposomes. The hydrated lipids were extensively mixed and vortexed for 5 min and then extruded 11 times through a polycarbonate membrane filter with a specific pore size, usually 100 or 200 nm, to form small unilamellar vesicles. The size distribution of the formed liposomes was measured using nanoparticle tracking analysis (NTA, NanoSight LM10, Malvern Instruments Ltm).

To prepare the immunoliposomes, liposomes containing 10% of a lipid with a maleimide group and a polyethylene glycol (PEG) spacer (DSPE-PEG(2000) Maleimide) were used. The chosen antibody was then prepared with a thiolating agent, called Traut's reagent (2-Iminothiolane), to convert primary amines on the antibodies into thiol groups. The thiolated antibodies were then added to the liposomes for conjugation using the reactivity of maleimide to thiol (Jølck et al. 2010; Nobs et al. 2004). After 1 hour of incubation, the antibody-liposome conjugation was discontinued by a filtration step, to separate the non-conjugated antibodies from the immunoliposomes. For this purpose, a gel column packed with

Sepharose-4B was used, to be able to separate the molecules according to size (so called size exclusion). The antibody-liposome mixture was added to the top of the column and eluted by rinsing with PBS. The eluted sample was collected into different fractions, containing 250 µl each, which were analyzed further with a spectrofluorometer to detect the liposomes (labeled with Rhodamine) and the antibodies (labeled with Alexa Fluor 430) in the different fractions. Since the liposomes are much larger than the antibodies, they were eluted in the first fractions, while the antibodies were retained by the porous network in the column and thereby efficiently separated from the liposomes. The fractions that were found to contain the immunoliposomes were pooled together and diluted to 0.5 mg/mL in PBS and stored at 4°C until use. An overview of the immunoliposome preparation protocol can be seen in Fig. 4.
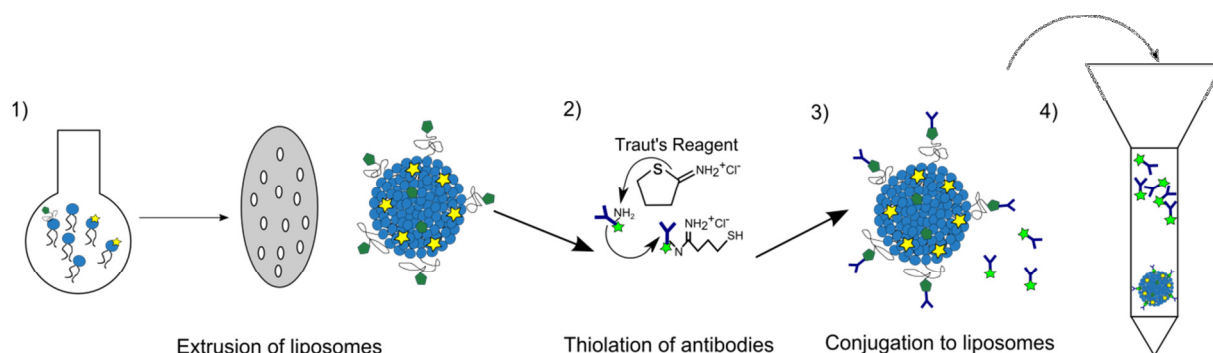

Figure 4 Schematic illustration of the preparation of immunoliposomes. (1) First the liposomes are made by extrusion of a hydrated lipid mixture, including a lipid with a PEGylated maleimide head group (green) and a fluorescently labeled lipid (yellow), through a polycarbonate membrane with defined pore size. (2) The antibodies are modified with Traut's reagent, to convert primary amines to thiol groups. (3) The antibodies are added to the liposomes to produce a stable conjugation of the thiols to the maleimide groups in the liposomes. The preparation protocol is finalized with a gel filtration step (4) to separate non-conjugated antibodies from the immunoliposomes by size exclusion.

3.2 QCM-D

QCM-D is a technique that can be used to measure the mass and viscoelastic properties of molecules adsorbing onto the surface of the quartz crystal sensor, by utilizing the piezoelectric properties of quartz (Höök et al. 1998; Rodahl et al. 1995). By applying an AC voltage, the crystal can be excited to oscillate at its resonance frequency. When molecules are adsorbed on the crystal surface, a shift in the resonance frequency (Δf) can be measured that depends on the change in mass on the sensor surface. Another parameter that is measured with QCM-D is the energy dissipation (ΔD), which represents the loss of energy from the sensor surface to the surrounding fluid and depends on the viscoelastic properties of the molecules on the surface. If the adsorbed molecular layer is very rigid, the energy dissipation is low ($\Delta D \sim 0$). In this case, the frequency shift is directly proportional to the molecular mass and the coupled solvent, according to the Sauerbrey relation (Sauerbrey 1959):

$$\Delta m \ = \frac{C}{n} \Delta f$$

where C is the mass-sensitivity constant (C = 17.7 ng/(cm^3 Hz) for quartz crystals with a fundamental resonance frequency of 5 MHz) and n is the overtone number (1, 3, 5...). Here, it is also assumed that (i) the added mass is small compared to the crystal mass, (ii) is distributed in a uniform layer on the surface and (iii) that the layer is attached under no-slip conditions during the oscillation. However, if the absorbed layer is less rigid, the molecules will form a soft film on the crystal surface that is deformed during the oscillation. The formation of these surfaces is characterized by high dissipation shifts ($\Delta D > 0$) and in this case the mass will not be directly proportional to the frequency shift. To estimate the adsorbed mass, the viscoelastic property needs to be accounted for, and therefore the Sauerbrey equation cannot be used. Instead a viscoelastic model can be applied; such as a Voight-based model (Voinova et al. 1999), by which the thickness, δ, or the density, ρ, of the adsorbed layer can be estimated. However, to solve the unknown parameters in this equation it is important to measure at different overtones simultaneously (Höök et al. 2001; Reimhult et al. 2002).

In comparison with other biosensing techniques, such as surface plasmon resonance, QCM-D does not only measure the mass of the adsorbed molecules on the sensor surface, but also the hydration and trapped water in the adsorbed layer (Bingen et al. 2008; Höök et al. 2001). This can be water trapped inside for example lipid vesicles, in between or underneath the molecules, or in any other way bound to the adsorbed molecular layer, such as hydrated

polymers chains. High amounts of trapped water typically increase the energy dissipation of the surface, but also rigid films (with low ΔD) can entrap significant amounts of water.

Besides using QCM-D to determine the mass or thickness of the adsorbed film of molecules, it can also be used to investigate different kinds of interactions on the sensor surface (Nilebäck et al. 2011; Speight and Cooper 2012), such as protein–protein interactions (Höök et al. 1998), DNA hybridization (Gunnarsson et al. 2008), virus attachment to lipid membranes and even for live cell studies (Frost et al. 2013; Tymchenko et al. 2013). It can also be used to monitor the adsorption of liposomes onto a surface and the subsequent formation of a supported lipid bilayer (Keller and Kasemo 1998). By investigating the frequency and dissipation shifts caused by sequential binding of different molecules to the surface, one can also distinguish different molecules from each other, depending on their viscoelastic properties on the surface. An example of the frequency and dissipation shifts obtained upon binding of different kinds of molecules to a model surface is shown in Fig. 5. Here, one can clearly see the difference in response, in particular in dissipation shift, when the large water-containing immunoliposomes (circles) bind to the surface in comparison to the binding of the much smaller and more rigid antibodies (squares).
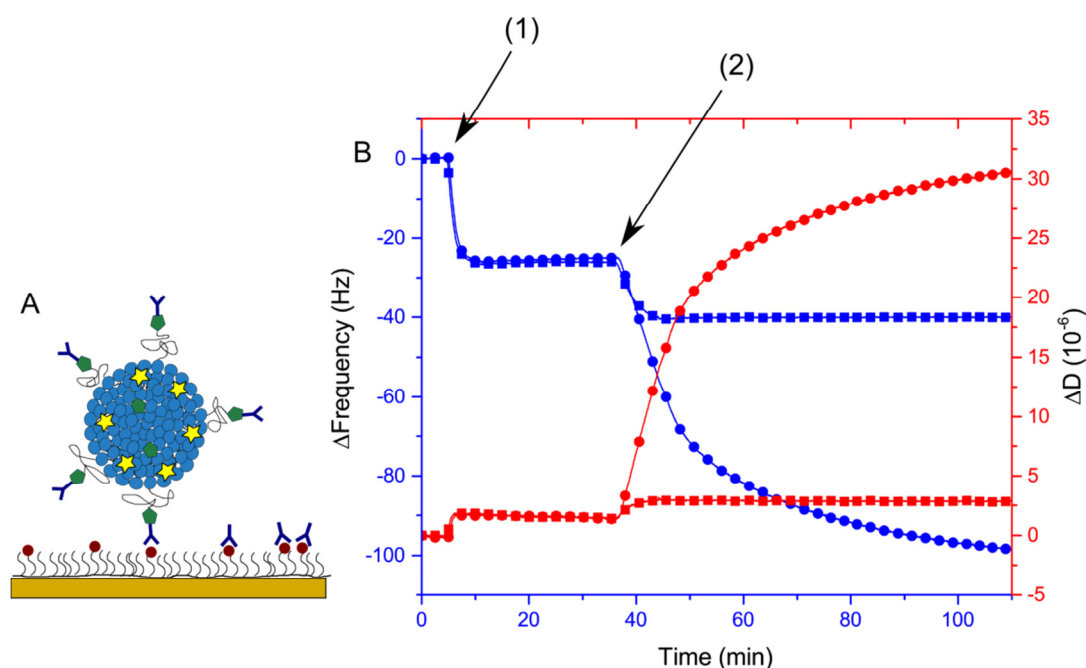

Figure 5 (A) A schematic illustration of an immunoliposome and antibodies binding to a model surface containing the biotinylated polymer PLLgPEG. (B) QCM-D graph showing the frequency (blue) and dissipation (red) shifts measured when different molecules are adsorbed on the quartz crystal surface; (1) PLLgPEG-biotin and (2) immunoliposomes (circles) versus antibodies (squares).

3.3 FLUORESCENCE MICROSCOPY

Fluorescence microscopy is a widespread method used for imaging of molecules in biological samples, such as living cells and tissue samples (Swedlow 2012). The basic principle behind the method is to use fluorophores as labels for the target of interest (Lichtman and Conchello 2005). Fluorophores are molecules with the ability to absorb and emit light at specific wavelengths. One example of a naturally occurring fluorescent molecule is the green fluorescent protein (GFP), which has been found in the jellyfish *Aequorea victoria* (Shimomura et al. 1962). Similar proteins have also been found in corals, and are extensively used today in biological studies for localization of specific proteins within the cell, by co-expressing the protein of interest with the GFP sequence, thereby creating an artificial tag within the cell (Chalfie et al. 1994).

There are many other biomolecules that possess fluorescent properties, and these molecules are referred to as intrinsic fluorophores. One example is aromatic amino acids, such as tryptophan, tyrosine and phenylalanine, which can absorb light in the UV range (260-295 nm) (Lakowicz 2006). Other common intrinsic fluorophores are enzyme cofactors, such as NADH and flavins. Also, common components of intact tissue have fluorescent properties, which are typically more dependent on the structure of the tissue than on specific fluorophores. These intrinsic fluorophores and structures often give rise to autofluorescence in the tissue. DNA and lipids, on the other hand, are often nonfluorescent. Some extrinsic fluorophores bind spontaneously to specific biomolecules and can therefore be used as probes. One example is 4',6-diamidino-2-phenylindole (DAPI), which binds selectively to DNA and can thus be used to stain the DNA-rich nuclei insides cells. In other cases, IHC can be used for labeling of specific molecules, as described in section 2.2.

Since different fluorophores emit light at different wavelengths, it is possible to use several fluorophores at the same time, allowing for simultaneous imaging of various molecules. However, it is only possible to use fluorophores that do not overlap each other in the excitation or emission spectra; otherwise the fluorescence signals cannot be distinguished from each other. This phenomenon of fluorescence interference between different fluorophores is called "cross-talk", and limits the use to 3-4 fluorophores at the same time for specific identification of each molecule, as visualized in figure 6. In this figure, one can also see that fluorophores with a broader excitation or emission spectrum, such as DAPI (blue), decreases the number of additional fluorophores that can be used at the same time. Therefore, new fluorophores are continuously developed to achieve as specific fluorescent markers as

possible and to increase the multiplexing capability. One such type is the recently developed Alexa Fluor dyes (Molecular probes, Invitrogen), which includes fluorophores that span all the way from near-UV to near-IR light. Besides the wide range of wavelengths, these new fluorophores are also less prone to photobleaching, which otherwise is a common disadvantage of fluorescent probes (Berlier et al. 2003).
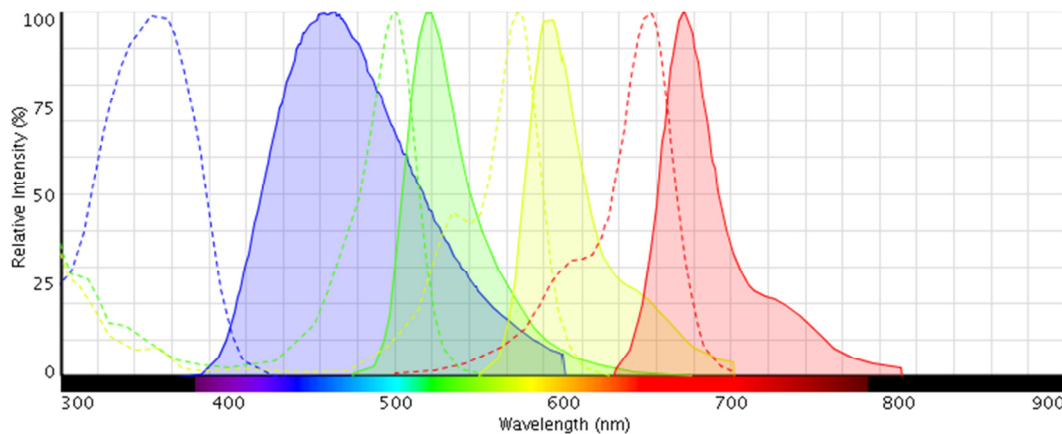

Figure 6 Normalized excitation (dotted lines) and emission (straight lines, filled curves) spectra of four different fluorophores, illustrating the potential risk of spectral overlap when using too many fluorophores at the same time. Blue = DAPI, green = Alexa Fluor 488, yellow = Rhodamine red, red = Alexa Fluor 647. The graph was created using the online tool Fluorescence SpectraViewer (ThermoFisherScientific 2016).

One of the greatest advantages of fluorescence microscopy, as compared to bright-field microscopy where the sample contrast is produced by absorbance of light in the sample, is the high contrast between the fluorescence signal and the background of the surrounding specimen. To be able to detect only the emitted fluorescence from the sample, conventional wide-field fluorescence microscopes are equipped with specific filter cubes that are specially designed for each fluorophore (Lichtman and Conchello 2005). The filter cube consists of three parts; an excitation filter, a dichroic mirror and a barrier (emission) filter. The excitation filter selects a specific wavelength from the light source that can pass to the specimen. The selected wavelength is directed to the sample using a dichroic mirror, which reflects the light onto the sample and, at the same time, allows selected emitted light of longer wavelength to pass through to the detector. In this way, the excitation light will not reach the detector. The emitted light from the sample that passes through the dichroic mirror is then further filtered by the barrier filter, which allows only specific wavelengths to pass through to the detector. Using different sets of filter cubes, the sample can be analyzed further for subsequent detection of different fluorophores in the sample. One way to increase the multiplexing capability, and to reduce cross-talk between the different fluorophores, is to choose narrow-

band filter cubes, which will allow only very narrow range of wavelengths to reach the detector. Of course, this will also result in lower signal from the fluorophores compared to using broad-band emission filters.

A disadvantage with the conventional wide-field fluorescence microscopy is the lack of ability to focus in depth of the tissue samples, resulting in blurred subcellular structures at high magnifications. The reason for this effect is that the collected light does not only originate from the focused field of view, but from the entire depth of the tissue. A solution to this problem is to use confocal microscopy (Smith 2008). In confocal microscopy, a small probe of light is focused by a laser beam and scanned through the sample at a very specific sample depth, called the optical section. Thus, only fluorophores in this specific volume are excited. The emitted light is then further filtered by passing through a small aperture, so-called pinhole, before reaching the detector, to exclude out-of-focus light. The resulting images thus display much higher contrast than what can be obtained with a wide-field microscope, however, at the cost of fluorescent signal intensity. Nevertheless, by scanning the sample multiple times at varying depth, 3D images of the sample can be constructed. Confocal microscopy can thus be of great advantage when imaging small structures in biological samples.

3.4 ToF-SIMS

ToF-SIMS is an analytical technique that can be used to analyze the chemical composition of analytes on a solid surface. By using a beam of ions, called primary ions, to bombard the sample, secondary ions specific to the sample surface are created (Benninghoven 1973). The emitted secondary ions are extracted by an electrostatic field into a time-of-flight analyzer where they are separated according to their mass versus charge-ratio (m/z) and detected to produce a mass spectrum (Chait and Standing 1981).

The primary ions are generated in an ion source, such as a liquid metal ion gun (LMIG), which extracts and focuses the ions into an ion beam (A. Brunelle et al. 2005). The primary ion beam is rastered over the sample surface to create secondary ions from different positions on the sample surface, thus collecting information about the molecular composition in each position. In the time-of-flight analyzer, the collected secondary ions are accelerated to the same kinetic energy and allowed to propagate in a field-free region, where they are separated according to m/z ratio, since ions with higher mass travel the distance with lower velocity than ions with lower mass.

The measured time of flight can be used to calculate the mass of extracted ions by using the formulas;

$$E = z \times U$$

$$E = \frac{mv^2}{2} \qquad v = \frac{L}{t} \qquad t = L\sqrt{\frac{m}{2zU}}$$

where m and v are the mass and velocity, respectively, and z is the charge (in most cases ± 1) of the secondary ion, whereas L is the length and U is the electrostatic potential (relative to the sample) of the time-of-flight analyzer (Vickerman and Briggs 2001). Thus, by measuring the time needed to reach the detector, the distribution of secondary ions can be visualized in a mass spectrum according to the m/z ratio. By selecting a peak in the mass spectrum that corresponds to a specific molecule, 2D images can be generated that show the signal intensity (that is, counts of secondary ions) of the selected ion in each position of the sample. A simplified illustration of the process is shown in figure 7.
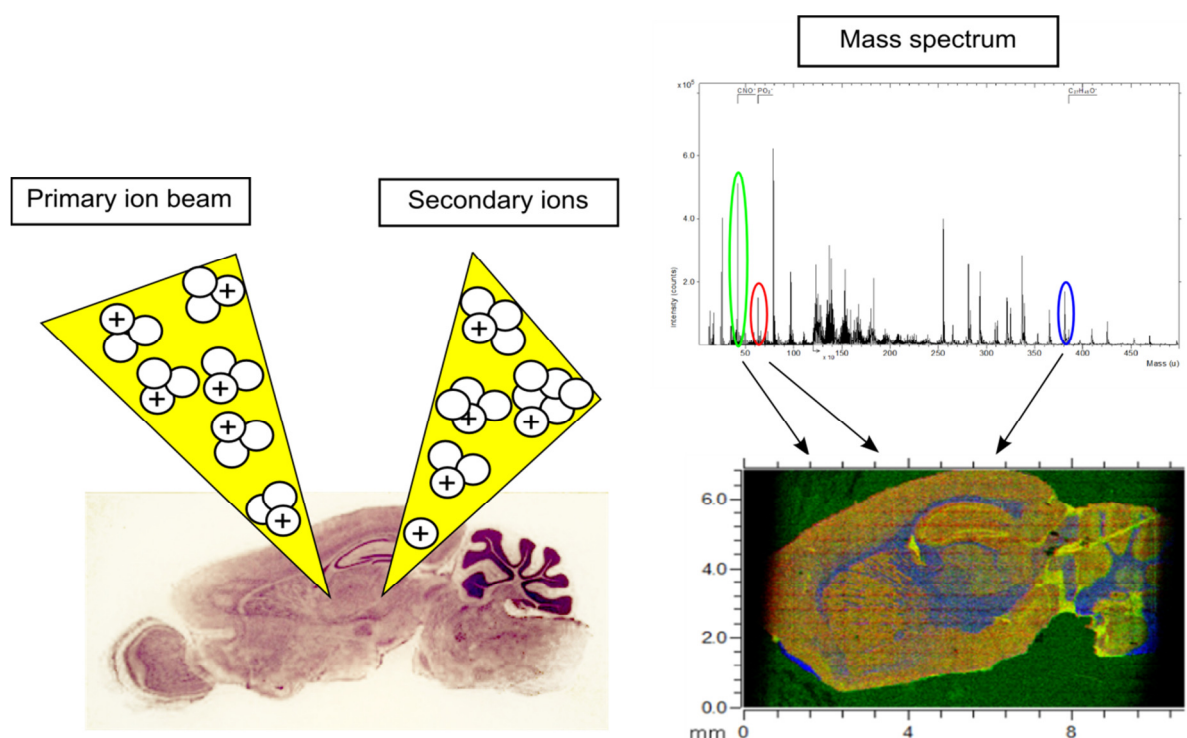

Figure 7 An illustration of the basic principle of ToF-SIMS imaging. An ion source generates a primary ion beam, which is focused onto the sample. As the sample is bombarded by the primary ions, secondary ions are formed and emitted from the surface. The emitted secondary ions are then collected and accelerated into a time-of-flight analyzer where they are separated according to mass versus charge (m/z) ratio and visualized in a mass spectrum. From this spectrum images can be generated, showing the spatial distribution of different molecules on the sample surface. In this example, an overlay image visualizing the distribution of PO_2^- (red), CNO^- (green) and cholesterol (blue) ions in a mouse brain section is shown.

The collision of primary ions on the sample surface results in extensive fragmentation of the molecules in the topmost layer (~10 nm) of the surface (Mas et al. 2008). A small percentage (< 1%) of the fragmented molecules is emitted from the surface as ions. Since the collision results in both negative and positive ions (as well as neutral molecular fragments), the sample is often analyzed twice, once for each polarity of the ions to be collected. Since the primary ions cause molecular damage on the surface of the sample, it is important that the surface area impacted by a specific primary ion, also referred to as the damage cross-section (σ), is only analyzed once to ensure a native sample surface. Therefore, analysis is often performed in the so called static mode, which means that very low doses of primary ions are used. The limit of primary ion dose density (PIDD) that can be used in this mode is called the static SIMS limit, and is proportional to the inverse of the damage cross-section (1/ σ), which depends on the type of primary ion used (A. Brunelle et al. 2005). However, it is generally stated that the PIDD should be lower than 10^{13} ions/cm^2 to ensure a native sample surface (Vickerman and Briggs 2001), even though surface damage effects, such as decrease in secondary ion yields, have been observed already at a PIDD of 10^{12} ions/cm^2 (Thiel and Sjovall 2015).

To avoid charging effects in insulating samples, including most biological samples, a pulsed low-energy electron flood gun is often used for charge compensation. The flood gun applies a current of electrons over the sample, in-between the pulses with primary ions, to neutralize the surface. The electron dose density is kept low to prevent damage to the surface. However, when analyzing a surface for a long time, electron induced surface modifications might occur and need to be accounted for (Gilmore and Seah 2002).

Cluster primary ion beams

A disadvantage with analysis in the static mode is a low yield of secondary ions. To improve the yield, cluster ions, such as Au_3^+ or Bi_3^+, are often used instead of the historically used monatomic ions, such as Ga^+ or In^+, as primary ion beams (A. Brunelle et al. 2005). Cluster ions have lower energy per constituent which results in less penetration of the sample and a more spread-out energy distribution in the topmost surface region of the sample. Cluster ions can therefore increase the yield of secondary ions from the surface, especially of molecular ions. Another advantage of using cluster ion beams is that the low penetration depth causes less molecular damage to the sample, enabling analysis beyond the static SIMS limit and even depth profiling of the sample, by using for example C_{60}^+ (Fletcher et al. 2007; Jones et al. 2007, 2008) or Argon (Ar_n^+, where n > 500) cluster ion beams, also referred to as gas cluster ion beams (GCIB) (Angerer et al. 2015a; Claudia Bich et al. 2013b; Shard et al. 2012;

Yamada et al. 2010). Another recently developed promising GCIB is the water-containing $((H_2O)_{6000}^+)$ cluster ion beam (Berrueta Razo et al. 2014). These larger cluster ion beams have shown to produce higher yield of molecular ions, especially of intact lipid molecules (~500-900 m/z) (Razo et al. 2015). However, these large cluster ion beams are also more difficult to focus, resulting in lower spatial resolution (~1 µm for C_{60}^+ and ~10 µm for the GCIB) (Razo et al. 2015). Therefore, these ion beams are often used in a dual-ion beam setting, where the large cluster ions are used to sputter off material from the surface, followed by imaging with a second ion beam, such as Bi_3^+ (Claudia Bich et al. 2013b; Breitenstein et al. 2007).

Mass resolution versus spatial resolution

ToF-SIMS can be used in different modes; either optimized for high mass resolution or for high spatial resolution (A. Brunelle et al. 2005; Mas et al. 2008). To obtain high mass resolution, a buncher is used to produce very short ion beam pulses. This mode produces spectra with narrow peaks, at a mass resolution of m/Δm up to ~10 000, allowing for effective separation of ions with similar mass. However, this mode also results in lower spatial resolution (~3-4 µm), since the short ion pulses are difficult to focus into smaller spots. To obtain high spatial resolution, longer pulses are used to produce more focused ion beams, resulting in a spatial resolution down to ~100 nm (Gunnarsson et al. 2010b). However, since the duration of pulses is longer, the peaks in the mass spectrum becomes wider, which might result in lower specificity of the detected ions.

In addition to the focus of the primary ion beam at the sample surface, the spatial resolution that can be obtained in the ion images is dependent on the so called useful lateral resolution (ΔL), which provides the surface area needed to detect a sufficient number (N) of secondary ions of the molecule of interest to be considered a significant signal (A. Brunelle et al. 2005). The useful lateral resolution is given by:

$$\Delta L^2 = \frac{N}{E} = \frac{N}{\left(Y/\sigma\right)}$$

where E is the detection efficiency (number of secondary ions per cm^2), Y is the secondary ion yield (number of secondary ions per primary ion) and σ is the disappearance (damage) cross-section, which is the mean area damaged by one primary ion. The useful lateral resolution is thus highly dependent on the investigated molecule, as well as the type of primary ion beam used in the analysis. For example, ΔL for cholesterol ions (m/z = 385) in a rat brain section was found to be ~500 nm using a Bi_3^+ primary ion beam at 25 keV (A. Brunelle et al. 2005),

whereas the phosphocholine ion (m/z = 184) in a supported lipid bilayer was found to have a ΔL of ~100 nm with similar settings (Gunnarsson et al. 2010b).

Matrix effects

There are many factors that influence the formation of secondary ions from the surface. The basic SIMS equation is:

$$I_m = I_p Y_m \alpha_m^\pm \theta_m \eta$$

where I_m is the secondary ion current of the species m, I_p is the primary ion current, Y is the sputter yield of secondary ions per primary ion impact, $\alpha^\pm$ is the ionization probability of a particular ion, θ is the fractional surface concentration of m and η is the transmission of the instrument (Vickerman and Briggs 2001). Thus, the emission of secondary ions is highly dependent on the properties of the species, and the surrounding chemical environment. The latter is referred to as the matrix effect. One example of problems that can occur with matrix effects is the occurrence of salt on the surface, which can suppress the emission of some molecular ions while other ions are enhanced (Jones et al. 2007; Robinson and Castner 2013). Other factors that might influence the emission of secondary ions is the occurrence of specific lipids on the surface, such as cholesterol or phosphatidylcholine, which can suppress or enhance the emission of other molecules in the surroundings (Angerer et al. 2015b; Jones et al. 2008; Razo et al. 2015). It is therefore important to investigate these factors in a controlled manner, to be able to make an estimate of the amount of a particular substance on the surface.

Sample preparation

One thing that is important to consider when imaging biological samples is the sample preparation. Since ToF-SIMS analysis is performed in an ultrahigh vacuum chamber, the sample has to be dried or frozen prior to analysis. If the sample contains a lot of salt, it can be valuable to rinse the sample in water or a volatile salt buffer, such as ammonium formate (AF), before analysis, to prevent the suppression of ions and the formation of salt adducts (Jones et al. 2007; Malm et al. 2009; Robinson and Castner 2013). To preserve wet samples, cryofixation is often used, which involves plunge-freezing (PF) and freeze-drying (FD). PF refers to freezing the sample very fast in for example liquid propane at −185°C. In this way, the water molecules in the sample will not form normal ice crystals, but instead amorphous, non-crystalline ice in a process called vitrification (Severs 2006). In this way, structural damage of the sample can be prevented. The sample then has to be freeze-dried slowly in a vacuum chamber at low temperatures (< −80°C) to allow the water molecules to sublimate

from the surface, before recrystallization starts to occur. However, if the sample does not contain much water, such as thin tissue sections, it might be enough to just freeze-dry the sample at room temperature prior to analysis.
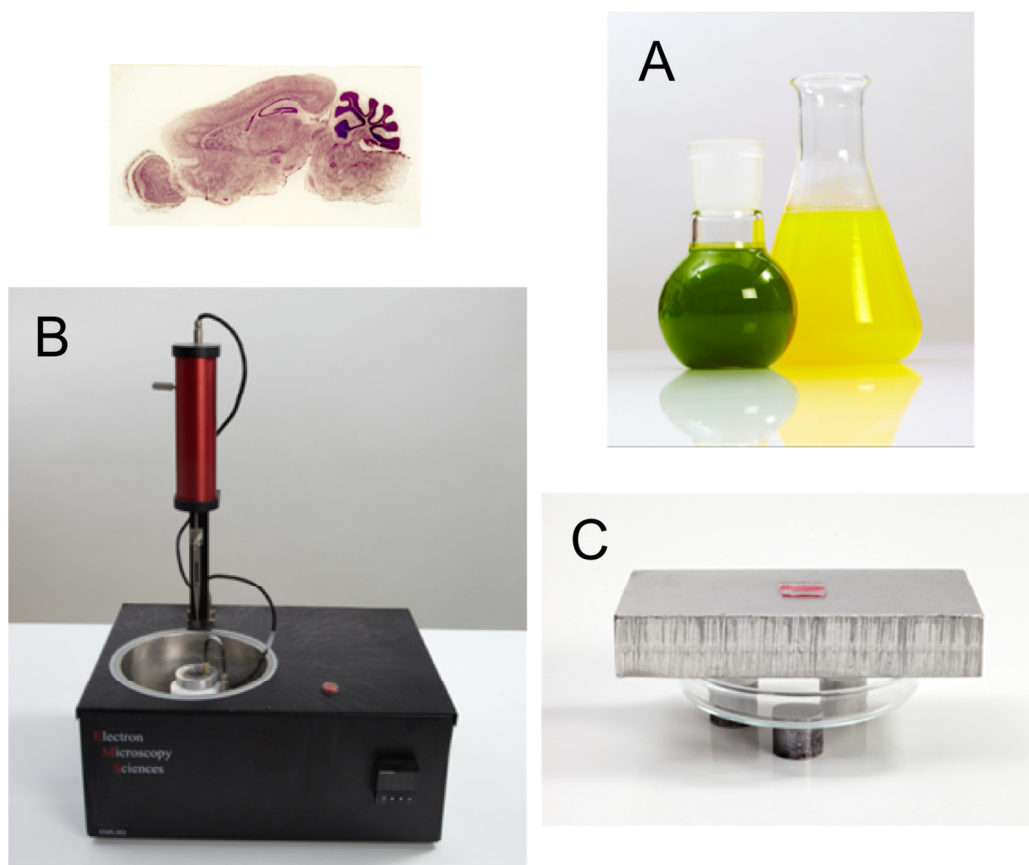

Figure 8 Illustration of the different steps that can be involved in the preparation of tissue samples prior to ToF-SIMS analysis; (A) rinsing with a volatile buffer, such as ammonium formate (note that the colors are just indicative of the liquid content and not representative of the color of the buffer), (B) plunge-freezing in liquid propane at −185°C, and (C) freeze-drying in vacuum chamber on a cold support.

3.5 MALDI

MALDI mass spectrometry is an IMS method that allows for detection and localization of different kinds of molecules in complex biological tissue samples (Caprioli et al. 1997; Chughtai and Heeren 2010; Pol et al. 2010; Rohner et al. 2005). The principle is similar to ToF-SIMS imaging, but instead of using a primary ion beam, the sample is irradiated with a laser beam. Furthermore, MALDI is based on embedding analytes of interest in a crystalline UV absorbing matrix that can absorb and transfer energy upon laser irradiation, leading to ion formation of the analytes. This results in very soft ionization of the molecules, with the formation of intact molecular ions in the range up to 100 kDa, and with nanomolar sensitivity (Benabdellah et al. 2010; Cornett et al. 2007). The desorbed and ionized molecules are then usually extracted and separated in a time-of-flight analyzer (as described in section 3.4), resulting in a mass spectrum with various peaks corresponding to the molecular mass of the molecules on the surface. By rastering the laser beam over the sample surface, 2D images can be created, showing the signal intensity of the detected molecules in each position of the sample.

Sample preparation

Sample preparation is of vital importance in MALDI. Depending on the type of molecule of interest, different preparations and matrices can be applied for optimal extraction of analytes. The matrix solution consists of the crystalline organic acid dissolved in an organic solvent and an additional acid, such as trifluoroacetic acid (TFA) or formic acid (Chughtai and Heeren 2010). The organic solvent, which often consists of ethanol, methanol or acetonitrile, is used to mix the matrix with extracted analytes from the sample and then evaporate from the surface, resulting in the formation of matrix crystals, including molecules from the sample, on the surface. By mixing the organic solvent in water, the evaporation rate can be tuned, allowing for slower crystal formation which affects the amount of analytes extracted from the surface. The concentration of the organic acid is another factor affecting the crystal formation and coverage on the surface. Higher concentrations results in greater crystal coverage on the surface but also faster crystal formation, which reduces the amount of extracted analytes. On the other hand, too low concentration of the organic acid results in too slow crystal formation, which may result in diffusion of analytes on the surfaces, thus affecting the spatial resolution. The purpose of the additional acid is to provide more protons to the desorbed molecules, thereby enhancing the ionization of the analytes.

The size and distribution of the matrix crystals is also dependent on the type of matrix used. One commonly used matrix is sinapinic acid (3,5-dimethoxy-4-hydroxycinnamic acid, SA), which has been shown to form evenly distributed crystals on the surface (Schwartz et al. 2003). Other commonly used matrices are 2,5-dihydroxybenxoic acid (DHB), which tend to form larger crystals, and α-cyano-4-hydroxycinnamic acid (CHCA), which forms more dense crystals (Cerruti et al. 2012; Schwartz et al. 2003). The choice of matrix mainly depends on the molecules of interest; SA is commonly used for molecules with higher molecular weight, such as proteins, whereas DHB and CHCA are used for extraction of analytes with lower molecular weight, such as lipids and peptides, respectively (Chughtai and Heeren 2010).

Another important preparation step when analyzing peptides and proteins is to wash the tissue section prior to matrix deposition, for removal of intrinsic salts and lipids that can interfere with the ionization process. This can be performed by immersing the tissue section briefly into different grades of ethanol, or other organic solvents, such as acetone and chloroform, or a volatile buffer such as ammonium formate (Martin-Lorenzo et al. 2014; Schwartz et al. 2003). This preparation step is thus not necessary when analyzing lipids in the tissue.

Furthermore, when using MALDI for imaging of biological samples, it is very important to apply the matrix in a proper way. Ideally, the matrix should result in small and clearly separated crystals, to prevent diffusion of analytes between the crystals and to achieve high spatial resolution. There are in principal two different techniques that can be used for this purpose; the first one is called spotting and the second spraying (Chughtai and Heeren 2010). In spotting, the matrix is applied as small droplet, either manually using for example a micropipette, or using automatic robotics, which can deposit picoliter sized droplets. However, even with the smallest droplets it is difficult to obtain smaller crystals than 100-200 µm with this method. Using a spraying device, the matrix is applied as mist upon the sample, resulting in a homogenous thin film of solid matrix crystal on the surface. In this way, crystals as small as 20 µm are formed, thus improving the capability for imaging with high spatial resolution. It is important to make sure that the sample is not wetted too much during the application, since this will increase the lateral diffusion of analytes on the surface. Therefore the matrix is often applied in cycles with repeating wetting and drying steps. A schematic illustration of the basic principles of MALDI imaging is shown in figure 9.
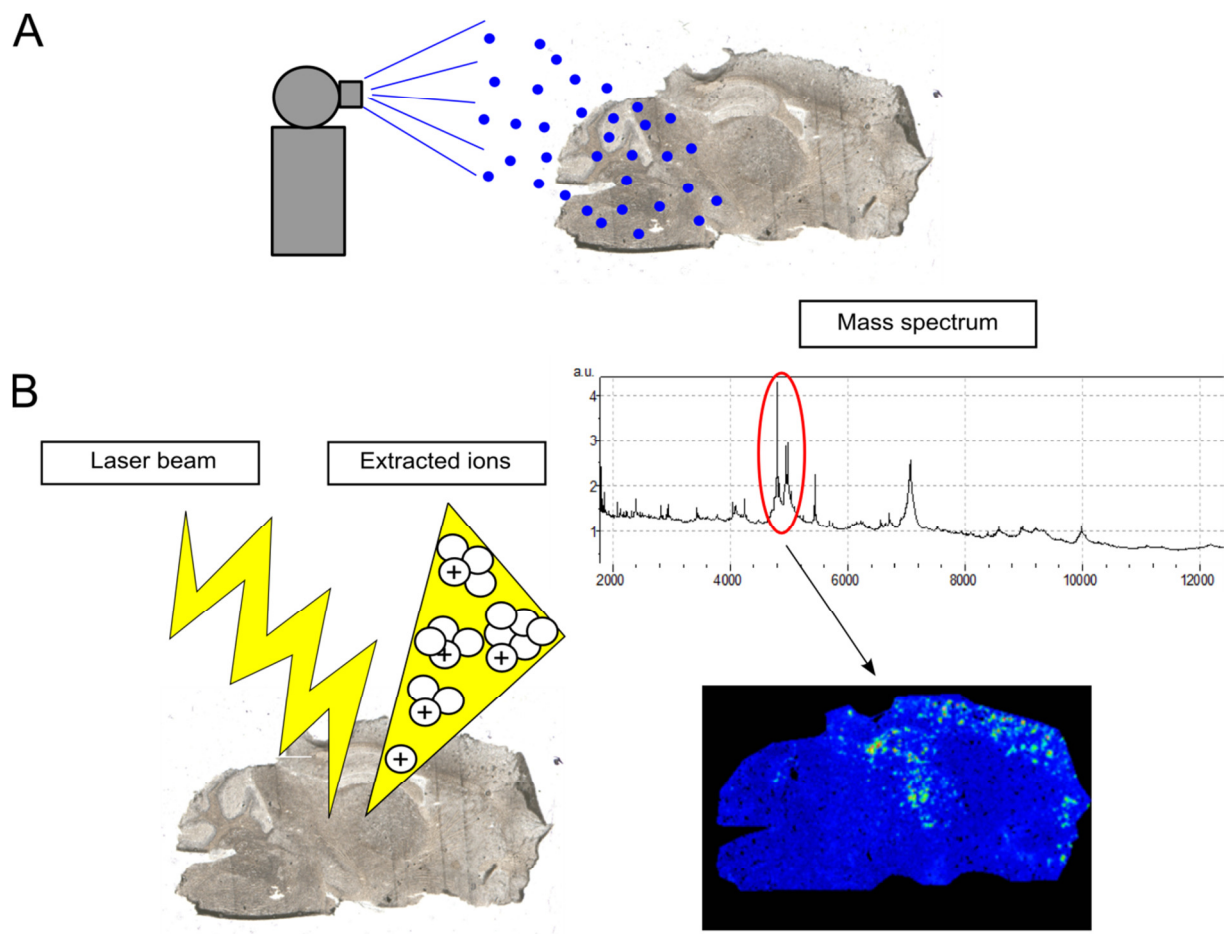
Figure 9 Schematic illustration of the basic principles of MALDI imaging, showing (A) the preparation of tissue sections by matrix application and (B) production of surface specific ions using a laser beam for imaging of specific molecules by choosing a specific peak (m/z) in mass spectrum.

4. SUMMARY OF RESULTS

In this section, a brief summary of the articles included in this thesis is presented and discussed. For more details, the reader is referred to the papers in the appendix.

PAPER I - LIPOSOME BINDING FOR MULTIPLEXED BIOMOLECULE DETECTION AND IMAGING USING TOF-SIMS

In paper I, the liposome approach for detection of biomolecules on surfaces was explored for the first time by detection of a single target, namely the protein neutravidin, at different concentrations on a model surface using biotinylated liposomes (Fig. 10A). For this purpose, the polymer PLLgPEG was used as a model surface, by mixing PLLgPEG at different ratios with biotinylated PLLgPEG, thereby creating model surfaces with different concentrations of biotin. Since neutravidin is a biotin-binding protein with four different binding sites, it can bind to the model surface and, at the same time, bind to other biotinylated molecules. In this way, biotinylated liposomes could be bound to the surface for subsequent detection with, for example, fluorescence microscopy and ToF-SIMS.

This model system was first evaluated using QCM-D, by which the frequency and dissipation shifts were measured upon sequential addition of each component to the surface, as shown in figure 10B. In this figure, one can clearly see how PLLgPEG-biotin/PLLgPEG is adsorbed to all surfaces, followed by adsorption of neutravidin at varying degrees, depending on the concentration of biotin (0.08-10%) on the surface. At the lowest biotin concentration, the adsorption is barely noticeable with QCM-D, neither by measuring the frequency or the dissipation shift. However, subsequent addition of the biotinylated liposomes results in a concentration dependent binding of the liposomes to all the model surfaces. The large shift in dissipation when the liposomes are added to the surface ((iii) in Fig. 10B) demonstrate the viscoelastic properties of the liposomes, which in this case serve as signal amplification at the lowest concentration on the surface (0.08%), where the frequency shift is barely noticeable.
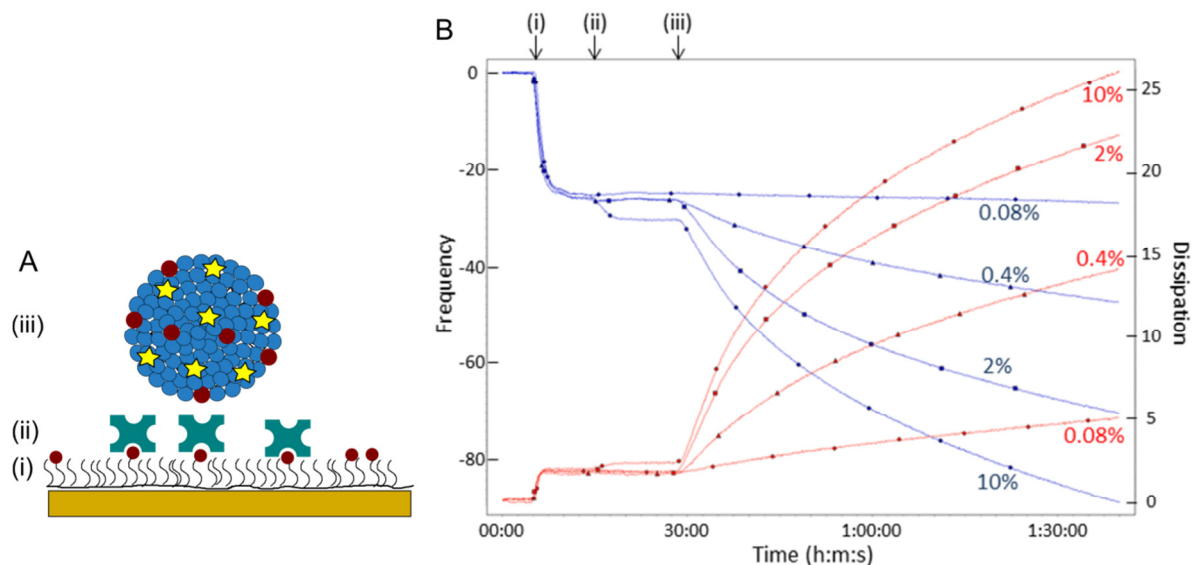
Figure 10 (A) Schematic illustration of the binding of biotinylated liposomes (iii) to a model surface containing PLLgPEG-biotin/PLLgPEG (i) and neutravidin (ii). (B) QCM-D graph showing the frequency (blue) and dissipation (red) shifts when binding each of the components to the model surface; (i) PLLgPEG-biotin/PLLgPEG, (ii) neutravidin and (iii) biotinylated liposomes, at different fractions of PLLgPEG-biotin (0.08%, 0.4%, 2% and 10%) on the surface. (B) is Reprinted with permission from (Sjövall et al. 2014). Copyright, 2014 John Wiley and Sons.

The same model system was used for detection of the liposomes at different concentration using fluorescence microscopy and ToF-SIMS imaging. For detection of the liposomes with fluorescence microscopy, fluorescently labeled lipids (DHPE-Rhodamine) were included in the liposomes. For specific detection with ToF-SIMS, deuterated phospholipids (D13-POPC) were used, which were easily detected by the different fragments of the phosphocholine head group in the mass spectrum (D13-PC$^+$, m/z = 66, 98, 117, 179, 197 and 237). Six model surfaces with different biotin concentrations, ranging from 0 to 10% PLLgPEG-biotin were investigated with fluorescence microscopy. The results show a clear concentration-dependent binding of the liposomes up to 0.5%, where saturation seems to occur. Furthermore, low non-specific binding (at 0% biotin) was detected. Similarly, ToF-SIMS analysis of model surfaces with 0 to 1% PLLgPEG-biotin showed a clear concentration dependency up to 0.5%. Also in this case, low non-specific binding was detected on the control surface (with 0% biotin), although it was found to be a bit higher than with fluorescence microscopy, indicating room for improvement of the preparation protocol. A graph summarizing the measured signal intensities of the liposomes detected with fluorescence microscopy and ToF-SIMS is presented in figure 11, showing similar biotin concentration dependencies for the two different imaging methods.
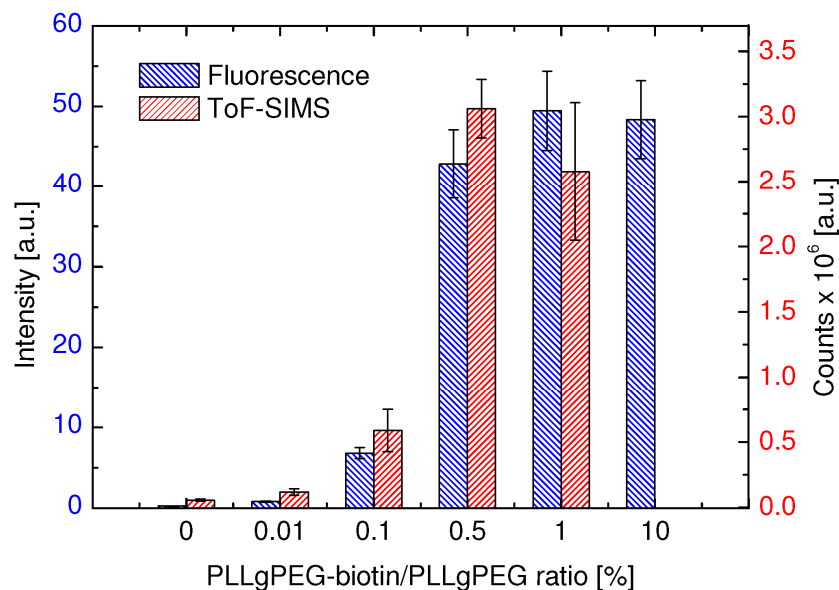
Figure 11 Graph showing the signal intensity (fluorescence intensities and ion counts, respectively) corresponding to liposome binding to model surfaces with different concentrations of PLLgPEG-biotin (0-10%), detected with fluorescence microscopy (blue) and ToF-SIMS (red). A clear concentration-dependency can be seen up to 0.5% PLLgPEG-biotin, where saturation seems to occur. Reprinted with permission from (Sjövall et al. 2014). Copyright 2014, John Wiley and Sons.

As the can be seen in figure 11, the liposome binding seems to saturate around, or maybe slightly below, 0.5% PLLgPEG-biotin, both with fluorescence and ToF-SIMS imaging. However, this saturation was not observed in the QCM-D measurement (Fig. 10), where the frequency and dissipation shifts continued to increase up to 10% surface-coverage of PLLgPEG-biotin. When calculating at which surface coverage there should be enough binding sites to form a full monolayer of liposomes, taking into account that each liposomes has a diameter of ~200 nm and that the surface area of each PLLgPEG-biotin molecule is ~100 nm^2, a saturation would be expected at ~0.3% PLLgPEG-biotin molecules on the surface (see paper I for more details). This thus correlates well with the observed saturation detected with fluorescence microscopy and ToF-SIMS, but not with QCM-D. This indicates that the adsorption detected by QCM-D at higher concentration corresponds to a thicker, or denser, liposome-layer than a single monolayer, which would not be detectable with fluorescence microscopy or ToF-SIMS after saturation. Since each neutravidin on the surface has four binding sites for biotin, there are, at most, three additional binding sites free for binding after binding to the model surface. This might result in binding of several liposomes to each neutravidin, even though this is not very likely considering the large size of the liposomes compared to neutravidin. Nevertheless, the fact that several liposomes can bind to each neutravidin on the surface, and also the opposite: that each biotinylated liposome

(containing over 1000 of biotin-tags) can bind to several neutravidin molecules, makes this liposome approach a bit tricky when trying to detect and quantify single molecules on the surface.

This liposome approach, using the biotin-avidin coupling, is also limited to a single target on the surface, and can thus not be used for multiplexed detection of different targets on the surface. Therefore, the liposome concept was developed further to include antibodies specific to the target of interest, instead of using the biotin-avidin coupling. These antibody-conjugated liposomes, also called immunoliposomes, were further explored in paper III, for detection of Amyloid-β, and in paper V, for multiplexed detection of both biotin and the glycosphingolipid GM1.

PAPER II - SIMULTANEOUS IMAGING OF AMYLOID-BETA AND LIPIDS IN BRAIN TISSUE USING ANTIBODY-COUPLED LIPOSOMES AND TIME-OF-FLIGHT SECONDARY ION MASS SPECTROMETRY

In the second paper, the liposome approach for detection of a single target using the biotin-avidin coupling was developed further to apply to a specific target, namely the peptide Aβ, in tissue sections from AD mouse brains. For this purpose, biotinylated antibodies specifically directed to Aβ was used, for subsequent binding of neutravidin and biotinylated liposomes (Fig. 12A). As described in paper I, the liposomes contained both fluorescently labeled lipids (DHPE-Rhodamine), and deuterated lipids (D13-POPC), for specific detection with fluorescence microscopy and ToF-SIMS, respectively. In this way, the same Aβ deposits could be detected in a region of the mouse brain (outlined by the square in Fig. 12B) with the antibody-coupled liposomes using both ToF-SIMS (Fig. 12C) and fluorescence microscopy (Fig.12E), showing very similar Aβ structures. Furthermore, investigation of the tissue section with optical (bright-field) microscopy, revealed very dense (dark) structures, indicating the presence of Aβ deposits (Fig. 12F). An adjacent control tissue section, subjected to the same preparation protocol but without the antibodies, was also investigated and did not reveal any significant nonspecific binding of the liposomes to the tissue in the same region of the mouse brain (Fig. 12D, the presence of Aβ is indicated by the circles). It could thus be concluded that the antibody-coupled liposomes bind specifically to Aβ deposits in the tissue sections.
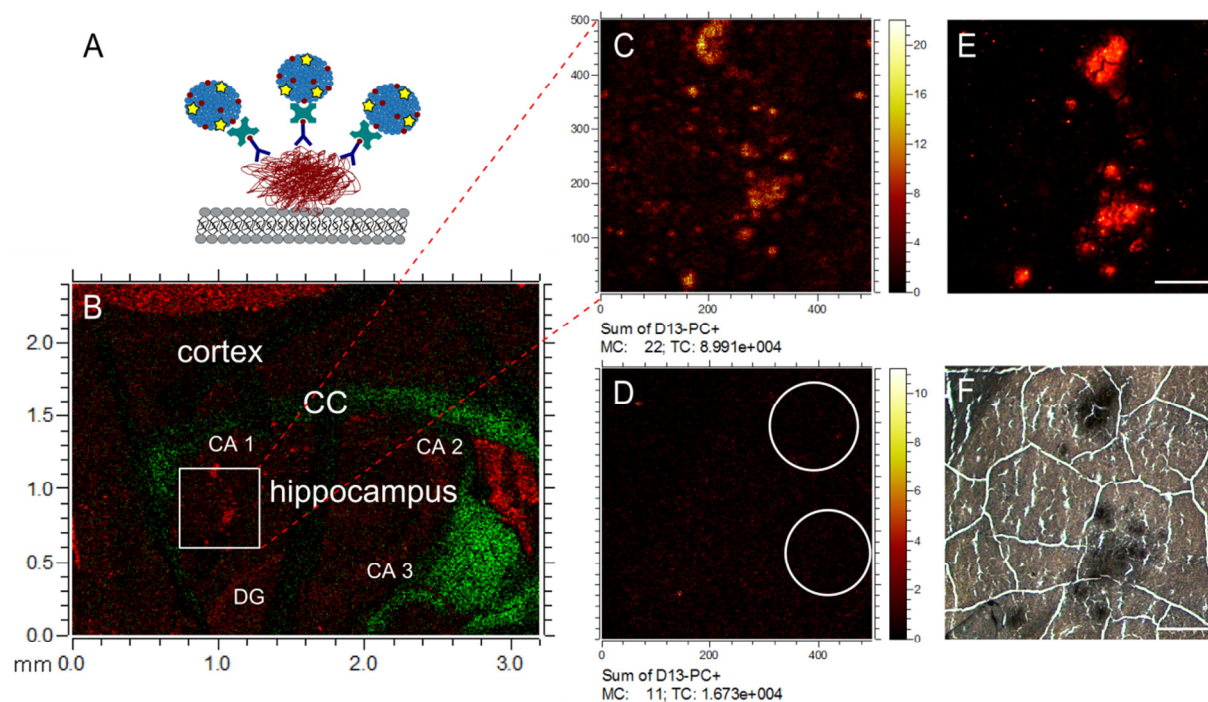
Figure 12 Imaging of Aβ in an AD mouse brain tissue section using antibody-coupled liposomes. (A) Schematic illustration of the detection principle using biotinylated antibodies specific to Aβ, followed by binding of neutravidin and biotinylated liposomes for subsequent detection with fluorescence microscopy and ToF-SIMS. (B) ToF-SIMS image of detected liposomes (red) and cholesterol ions (green) in a region of the mouse brain containing the hippocampus and cortex. CC = corpus callosum, DG = dentate gyrus, CA1, CA2 and CA3 = subregions in hippocampus. (C, E) Image of detected liposomes in the hippocampal area (visualized by the square in B) detected with ToF-SIMS (C) and fluorescence microscopy (E). (D) ToF-SIMS image of an adjacent tissue section incubated with the liposomes but without the antibodies (negative control). (F) Optical image (bright-field) of the same tissue section and region as (E). D13-PC+ = liposomes, MC = maximum counts in one pixel, TC = total counts. Scale bar = 100 µm. Reprinted with permission from (Carlred et al. 2014). Copyright 2014, American Chemical Society.

The aim of this study was not only to detect Aβ with ToF-SIMS, but also to image different lipids in parallel to Aβ. Since the liposomes were made of deuterated phospholipids, it was possible to image the native phospholipids in the surrounding tissue. Also, other lipids, such as cholesterol and sulfatides were successfully imaged in the vicinity of the Aβ deposits, revealing mostly complementary distribution patterns, although, some enrichment of sulfatides was observed close to some of the deposits (Fig. 13).
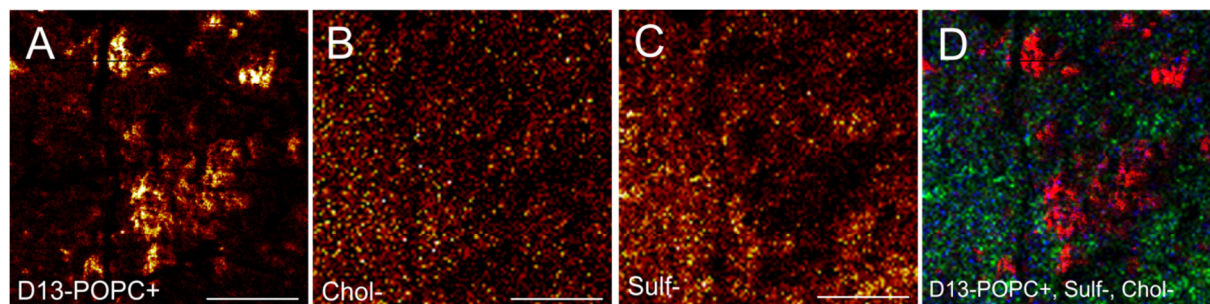
Figure 13 Simultaneous imaging of Aβ and lipids in an AD mouse brain tissue section using antibody-coupled liposomes and ToF-SIMS. ToF-SIMS images showing the distribution of (A) Aβ-bound liposomes (D13-POPC+), (B) cholesterol (Chol-) and (C) sulfatide (Sulf-) ions. (D) Overlay image of liposomes (red), sulfatides (green) and cholesterol (blue). Scale bar = 50 µm. Reprinted with permission from (Carlred et al. 2014). Copyright 2014, American Chemical Society.

However, when analyzing the spatial distribution of different biomolecules, and in particular lipids, it is of vital importance to make sure that the preparation protocol does not interfere with the sample integrity in some way. Several previous studies have shown that lipid migration might occur when raising the temperature of the sample (Sjövall et al. 2006), or when using fixatives or different kinds of rinsing buffers (C. Bich et al. 2013a; Malm et al. 2009). Therefore, the effects of the preparation protocol used in this approach were carefully investigated, by first analyzing the untreated tissue section in frozen state (at −80°C), and then once again after the preparation of the tissue, at room temperature (RT). For this purpose, an easily recognizable area (corpus callosum) of the mouse brain was selected and analyzed both before and after antibody/liposome preparation (Fig. 14). The resulting ion images clearly show an enhanced yield of lipid ions of the treated sample, but no lateral redistribution could be observed for the selected lipids. The increased ion yield might be explained by a combination of the raised temperature during the preparation, and by changes in the chemical environment, since the rinsing buffer used in the protocol (ammonium formate) is known to remove salt from the surface, which otherwise is known to suppress the ionization probability. Also, the spectrum of the prepared tissue section did not contain any additional unexpected peaks, such as artifacts from the preparation (see supporting information in paper II). Thus, it was concluded that the preparation protocol used in this approach does not generate major modifications of the lateral lipid distributions.
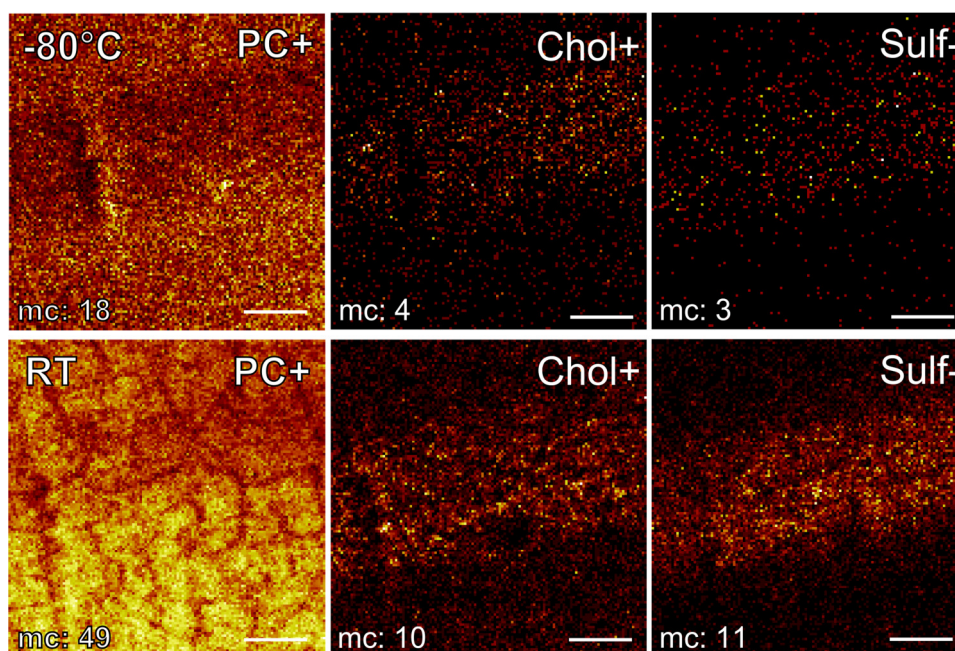
Figure 14 ToF-SIMS ion images showing the distribution of phosphatidylcholine (PC+), cholesterol (Chol+) and sulfatides (Sulf-) in the corpus callosum of an untreated mouse brain section, analyzed at −80°C (upper row), and in the same brain region after antibody/liposome preparation, analyzed at room temperature (RT) (lower row). mc = maximum counts in one pixel. Scale bar = 100 µm. Reprinted with permission from (Carlred et al. 2014). Copyright 2014, American Chemical Society.

PAPER III - IMAGING OF AMYLOID-BETA IN ALZHEIMER'S DISEASE TRANSGENIC MOUSE BRAINS WITH TIME-OF-FLIGHT SECONDARY ION MASS SPECTROMETRY USING IMMUNOLIPOSOMES

In this paper, the liposome approach for detection of specific molecules in tissue sections was developed further by using antibody-conjugated liposomes, so called immunoliposomes. The selected target molecule was again Aβ in AD mouse brains, in order to provide a proof-of-principle of the method in relation to previously published results (paper II). By using different antibodies and conjugating each of these to liposomes with a unique lipid composition, this approach opens up for the possibility to detect many different targets at the same time, at sensitivities on the single-molecule level.

The specificity of the immunoliposome binding to Aβ was first evaluated on a model surface, consisting of PLLgPEG-biotin, neutravidin and biotinylated Aβ, using QCM-D (Fig. 15). In this graph, the adsorption/binding of each component to the surface can be clearly observed by the shifts in frequency (blue) and dissipation (red). The addition of immunoliposomes ((iv) in Fig. 15B) is indicated by large shifts in both frequency and dissipation, which is typical for liposome adsorption and depends on their inherent viscoelastic properties (Höök et al. 2001). As a control, the immunoliposomes were also added to another model surface without Aβ on

the surface (dotted lines in Fig. 15B) and the results showed no binding of the immunoliposomes to the surface, demonstrating specific binding of the immunoliposomes to Aβ.
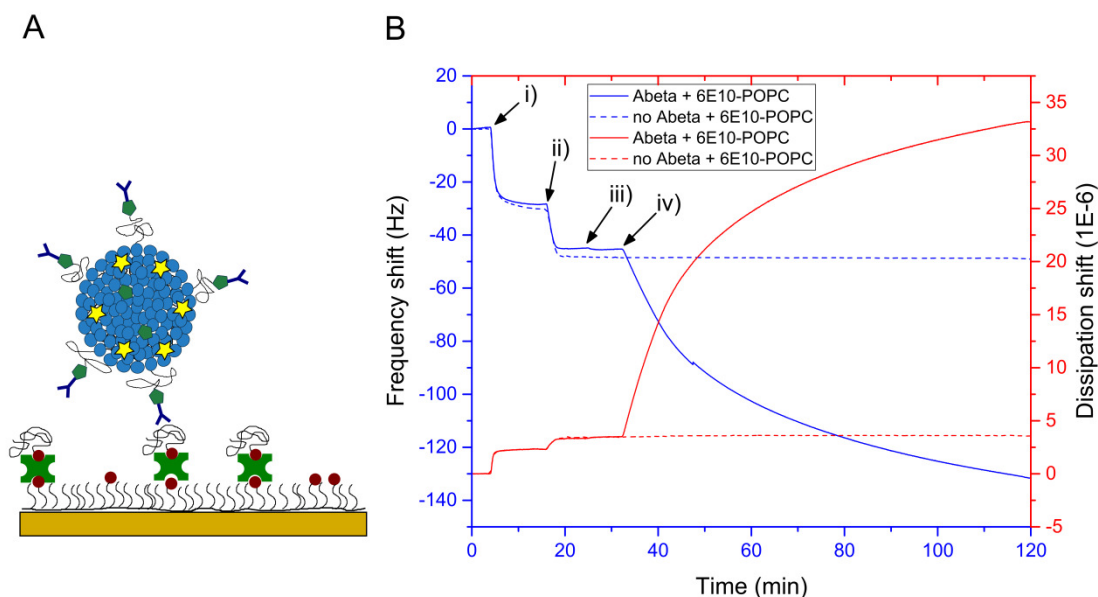

Figure 15 (A) Schematic illustration of the binding of an immunoliposome to biotinylated Aβ on a model surface consisting of PLLgPEG-biotin and neutravidin. (B) QCM-D graph showing the shifts in frequency (blue) and dissipation (red) when each of the components of the model surface is added to the quartz crystal sensor surface; (i) PLLgPEG-biotin, (ii) neutravidin, (iii) biotinylated Aβ (Abeta) and (iv) immunoliposomes (6E10-POPC). The dotted curves show adsorption of each component to a model surface where Aβ was omitted (no Abeta), as a control of nonspecific binding of the immunoliposomes to the surface. Reprinted with permission from (Carlred et al. 2016a). Copyright 2016, American Vacuum Society.

The immunoliposomes were further applied to tissue sections and investigated with fluorescence microscopy and ToF-SIMS for detection of Aβ deposits in the mouse brain. As an additional control, adjacent tissue sections were also stained with conventional IHC (that is, using primary and secondary antibodies), to compare with the immunoliposome-stained tissue sections. An example of the acquired ToF-SIMS and fluorescence images is shown in figure 16, which shows an Aβ deposit in the cortical region of the mouse brain, revealed by immunoliposome binding for subsequent detection with ToF-SIMS (Fig. 16B) or fluorescence microscopy (Fig. 16C-D). Figure 16A shows the total ion signal in the same region of the tissue sample analyzed before any preparations (untreated), revealing some topographic effects in the Aβ-affected area.
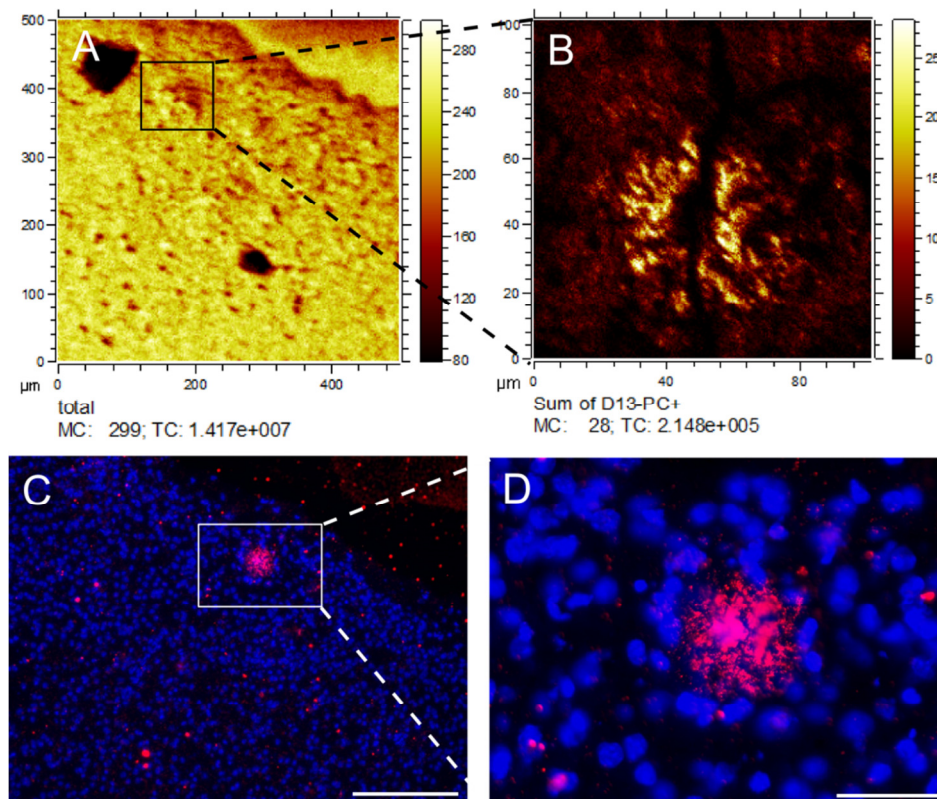
Figure 16 Localization of Aβ deposits in an AD mouse brain section using immunoliposomes. (A-B) ToF-SIMS images showing (A) the total (+) ion image of the untreated tissue sample indicating some topographic features in the cortical region of the mouse brain. (B) ToF-SIMS high resolution ion image of the same tissue section and region as in (A) but after incubation with immunoliposomes, showing the immunoliposome-signal (D13-PC+) from the region outlined by the square in (A). (C-D) Fluorescence images of the same tissue sample as (A-B) visualizing the binding of immunoliposomes (red) to an Aβ deposit at (C) 10× magnification (scale bar = 200 µm) and (D) at 40× magnification (scale bar = 50 µm). Cell nuclei are counterstained with DAPI (blue). Reprinted with permission from (Carlred et al. 2016a). Copyright 2016, American Vacuum Society.

Using the immunoliposome approach, Aβ and surrounding molecules can be investigated at the same time. In this way, several lipids, such as phosphatidylcholine, cholesterol, sulfatides and palmitic acid, were detected in the vicinity of the Aβ deposit (Fig. 17). Most of these lipids showed a complementary distribution to the Aβ deposit, although the sulfatides and palmitic acid displayed some colocalization with Aβ (Fig. 17D-F). Since the palmitic acid is a component of the fatty acids included in liposomes (POPC), this colocalization might be an artifact from the immunoliposomes, whereas the presence of sulfatides, in combination with cholesterol, might be an indication of degenerative processes in the myelin sheaths (that surrounds the axons of the nerve cells). These processes are highly relevant for the generation of AD pathology and needs further attention.
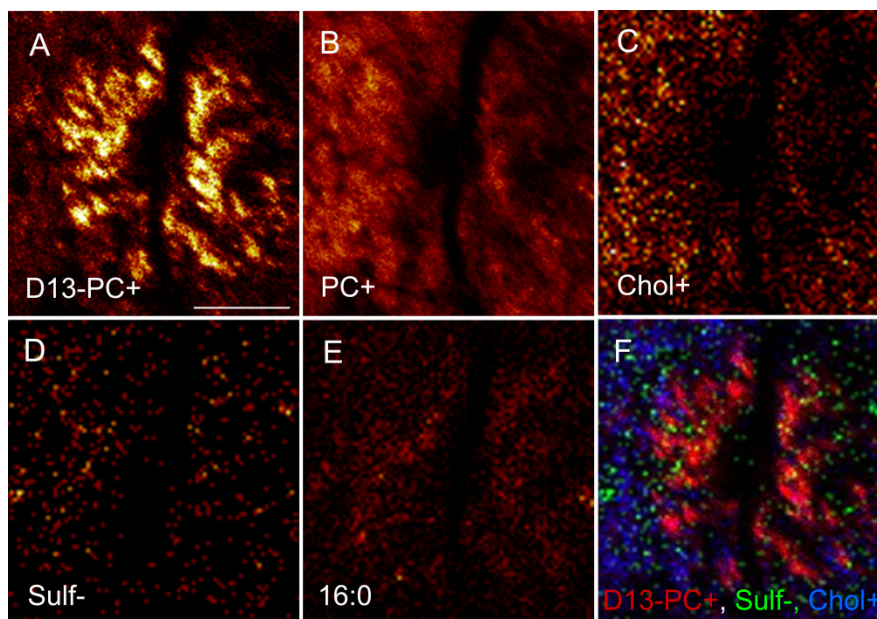
Figure 17 (A-E) ToF-SIMS high resolution ion images of (A) Aβ-bound immunoliposomes (D13-PC+), (B) phosphatidylcholine (PC+), (C) cholesterol (Chol+), (D) sulfatides (Sulf-) and (E) palmitic acid (16:0). (F) Overlay image of liposomes (red), sulfatides (green) and cholesterol (blue). Scale bar = 20 µm. Reprinted with permission from (Carlred et al. 2016a). Copyright 2016, American Vacuum Society.

As described in paper II, it is of vital importance to investigate possible effects of the preparation protocol on the sample integrity. Therefore, even though the sample preparation procedure is almost the same as in paper II, a tissue sample was analyzed with ToF-SIMS, before preparation (untreated, at room temperature) and then once again in the same region after incubation with the immunoliposomes. The results showed that the overall lipid distributions did not change considerably by the treatment. However, the secondary ion yield decreased significantly for almost all of the analyzed lipids (to ~15-25% of the untreated sample), except for the sulfatides, which increased with almost 160%. The effect was most prominent in the white matter of corpus callosum, where the cholesterol signal was significantly reduced and the sulfatides highly increased after liposome preparation, compared to the other brain regions.

These results are in contrast to our previous findings, in paper II, where it was found that all lipid signals were increased by the sample preparation. However, an important difference between the two studies is that the previous compared the ion yields with a sample in frozen state (at −80°C), while in this study the untreated sample was analyzed at room temperature (freeze-dried), thus removing the temperature aspect between the treated and untreated sample. It is therefore possible that the increased ion yields that were observed in the previous study were mainly caused by the elevated temperature, which might induce lipid migration to

the surface (Sjövall et al. 2006). By preventing or reversing this migration with the preparations in this study, enrichment of specific lipids, such as cholesterol, on the sample surface can be prevented. This, in turn, enables for the detection of other lipids on the surface, such as the sulfatides, which otherwise might be suppressed by the presence of cholesterol. A similar finding was discovered in a study by Angerer et al., in which the treatment of the tissue section with trifluoroacetic acid (TFA) reduced the cholesterol accumulation on the surface but enhanced the yields of many other lipids (Angerer et al. 2015b).

PAPER IV - PROBING CEREBRAL AMYLOID-BETA PATHOLOGY IN TRANSGENIC ALZHEIMER'S DISEASE (ARCSWE) MICE USING MALDI IMAGING MASS SPECTROMETRY

In this paper, another IMS technique was used to investigate the Aβ composition and distribution in AD mouse brains. For this purpose, a MALDI-TOF IMS instrument was used, which offers the possibility to investigate the distribution of peptides and proteins in the tissue. A challenge with MALDI IMS is the sample preparation, which needs to be optimized for each type of sample and analyte (as described in section 3.5). Since Aβ is a small peptide with a molecular mass of ~4 kDa, CHCA was chosen as the matrix. Imaging in the range of m/z 2-20 kDa and with a lateral resolution of ~50 µm resulted in a broad distribution of peaks. In particular, several interesting peaks at m/z ~4000-4500 displayed a very distinct spotty distribution pattern in the mouse brain, especially in the hippocampus and cortex. The data was further analyzed using multivariate statistics to identify the peaks that were localized to these distinct spots. Not surprisingly, several of the observed peaks at m/z ~ 4000-4500, but also some peaks at m/z 6000-6500, were found to cluster together at these locations. In particular, several peaks corresponding to the m/z of different Aβ peptides, such as Aβ(1-37), Aβ(1-38) and Aβ(1-40), where the number denotes the number of amino acids in the peptide, were strongly associated to these spots. To verify that these peaks indeed correspond to Aβ peptides, IHC (using primary and secondary antibodies) was performed on the same tissue section after the MALDI analysis (Fig. 18). The resulting images showed clear colocalization patterns of Aβ, visualized with fluorescence microscopy (Fig. 18B-C), and the MALDI single ion images (Fig. 18D-F), demonstrating that these peaks corresponds to Aβ deposits.
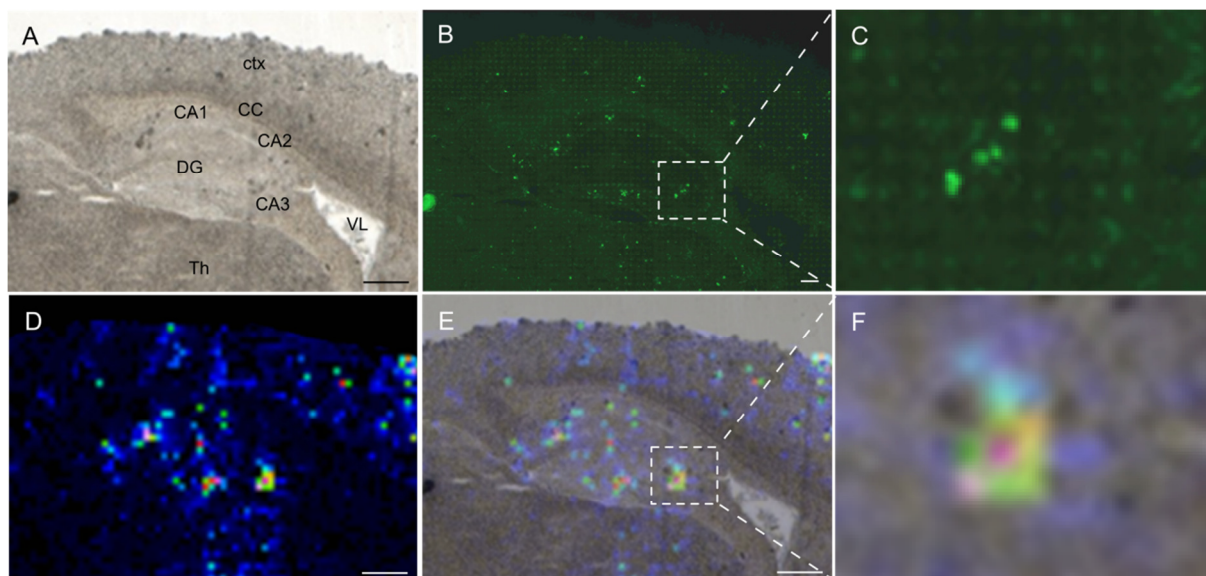
Figure 18 Detection of Aβ deposits in an AD mouse brain using MALDI IMS. (A) Optical image of selected regions in the mouse brain, containing the hippocampus and cortex (ctx). CC = corpus callosum, DG = dentate gyrus, CA1, CA2 and CA3 = subregions in hippocampus, Th = thalamus, VL = left ventricle. Scale bar = 1 mm. (B-C) Fluorescence images of the same region as in (A), showing the distribution of Aβ, immunostained using primary (6E10) and secondary (goat anti-mouse Alexa Fluor 488) antibodies at low (B) and high (C) magnification of the region outlined by the square in (B). Scale bar = 200 µm. (D) MALDI single ion image of the peak corresponding to Aβ(1-40) peptides, showing the distribution of Aβ deposits in the same mouse brain as in (A-C). (E-F) Overlay image of the optical image in (A) and the ion image in (D), showing the location of Aβ in the cortical and hippocampal regions of the mouse brain at low (E) and high (F) magnification of the selected region outlined by the square in (E). Scale bar = 1 mm. Reprinted with permission from (Carlred et al. 2016b). Copyright 2016, John Wiley and Sons.

To further investigate and validate the identity of the peaks at *m/z* 4000-4500, the deposits were analyzed using laser microdissection pressure catapulting (LMPC), which allows for collection of sample material from very specific areas in the tissue, followed by MALDI MS and MS/MS analysis. The resulting mass spectra clearly identified the previously observed peaks as Aβ(1-37), Aβ(1-38) and Aβ(1-40), as well as the Aβ(1-39) and Aβ(1-42) peptides (Fig. 19).
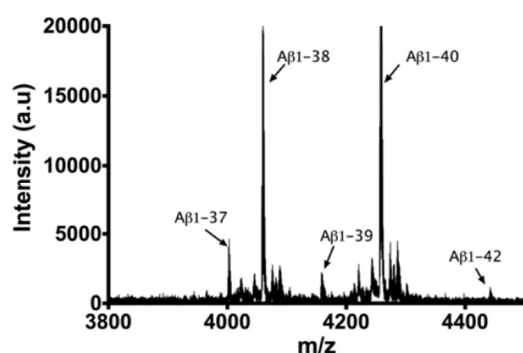

Figure 19 Acquired mass spectrum from MALDI MS analysis of individual Aβ deposits, collected using LMPC. Reprinted with permission from (Carlred et al. 2016b). Copyright 2016, John Wiley and Sons.

The imaged Aβ deposits were further analyzed with statistical methods by collecting spectral data from these localized spots in different regions of the mouse brain, including the hippocampus, the somatosensory cortex and the somatomotor cortex, and comparing the spectra with data from adjacent regions (control) in the same tissue section, to reveal any region-specific Aβ composition. The results showed that several Aβ peptides, including Aβ(1-38) and Aβ(1-40), were specifically localized to the deposits in all of the analyzed regions. Aβ(1-42), on the other hand, was only localized to the deposits in hippocampus and somatosensory cortex, whereas somatomotor cortex displayed a more dispersed distribution of this peptide. This finding indicates that this particular peptide, Aβ(1-42), has not been cleared from the nerve cells within this region yet, and might therefore be involved in intracellular neurodegenerative processes. However, more studies are needed to further evaluate this hypothesis; especially analysis on mouse brains at different ages would be helpful to reveal the Aβ generation and deposition.

Furthermore, several unknown peaks, many of them in the range of *m/z* 6000-6500, were found to be associated to the Aβ deposits. One of these peaks, at *m/z* 6175, which was localized to the hippocampal Aβ deposits (Fig. 20), was putatively recognized as the microphage migration inhibitory factor (MIF), according to previous findings (Rahman et al. 2011). To further investigate and validate the identity of this peak, IHC was performed, using antibodies directed to Aβ, MIF and also ionized calcium binding adaptor molecule 1 (Iba1), which is a marker for activated microglia. The resulting fluorescence images clearly showed colocalization of Aβ, MIF and Iba1 in the hippocampus. This thus indicates that the peak at *m/z* 6175 indeed corresponds to MIF, suggesting the involvement of activated inflammatory processes in AD pathology.
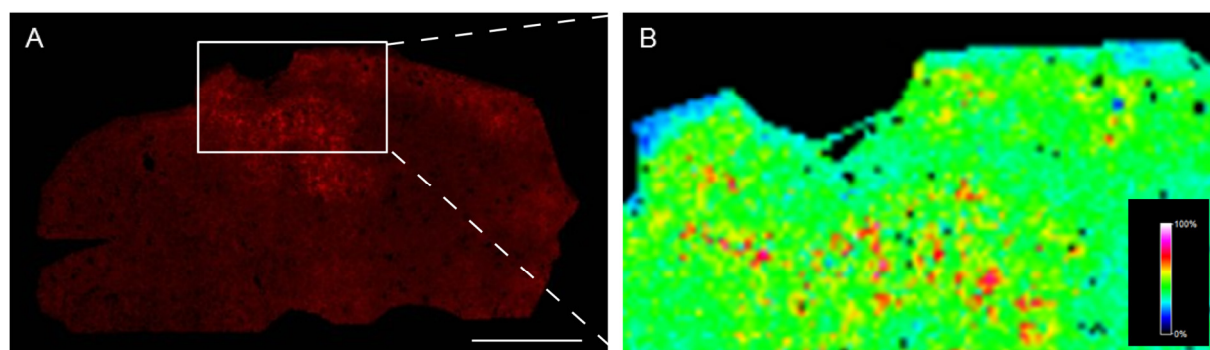

Figure 20 (A) MALDI image of ion peak at *m/z* 6175 (red), putatively assigned to MIF, and (B) higher magnification of the hippocampal region showing the accumulation of MIF in the hippocampal region. The color palette in the figure indicates signal intensities from 0-100%. Scale bar = 500 μm. Reprinted with permission from (Carlred et al. 2016b). Copyright 2016, John Wiley and Sons.

PAPER V - LIPOSOME APPROACH FOR MULTIPLEXED QUANTIFICATION OF BIOMOLECULES AT SURFACES USING TIME-OF-FLIGHT SECONDARY ION MASS SPECTROMETRY

In this paper, the liposome approach for detection of molecules on surfaces was developed further for detection and quantification of multiple targets on a model surface using immunoliposomes (as described in section 3.1 and in paper III). As a first step, the immunoliposomes, conjugated with antibiotin antibodies, were studied on model surfaces containing different concentrations PLLgPEG-biotin, to investigate specific binding and to determine the ability to quantify target concentrations on the surface. The immunoliposome binding was first investigated using QCM-D, on four model surfaces with different fractions PLLgPEG-biotin/PLLgPEG (0.08, 0.4, 2 and 10%). The results show a clear concentration dependent binding of the immunoliposomes to the surface (for further details, see Fig. 3 in paper V). The immunoliposome binding to different PLLgPEG-biotin (0-1%) surfaces was also investigated with fluorescence microscopy and ToF-SIMS, revealing a clear concentration dependent binding. Individual liposomes were clearly distinguishable in the images using both methods up to ~0.5% PLLgPEG-biotin, above which the liposomes were too close to be detected as individual entities.

To be able to include multiple targets on the surface, another model surface was used, namely supported lipid bilayers (SLB). The SLBs were formed by fusion of liposomes adsorbed on the surface. By choosing the lipid content in the liposomes, different tags or recognition elements was included, which thus were presented on the surface of the SLB. The model surface was first studied by including biotinylated lipids in the SLB, to investigate specific binding of the antibiotin immunoliposomes to the surface. The second investigated target was the glycosphingolipid GM1, which is known to bind strongly with Cholera toxin subunit B (Chtx) (Merritt et al. 1994). Thus, GM1 was included in the SLB, while Chtx was conjugated to liposomes. To be able to distinguish between the antibiotin and the Chtx liposomes, different deuterated phospholipids were used (D4 and D13-POPC), as well as different fluorophores (ATTO 488 and Rhodamine), in the liposomes. The binding of antibiotin and Chtx liposomes to the two different targets was first investigated separately using QCM-D, which displayed good specific binding of both liposomes to the model surface. It was noted, however, that some nonspecific binding occurred to the surface as well, although it was considered to be small compared to the specific binding (see Fig. 4 in paper V).

The simultaneous binding of liposomes to two different targets was investigated further by detection with fluorescence microscopy and ToF-SIMS. For this purpose, the different targets were incorporated into the SLB by mixing POPC liposomes containing one of the targets (biotin or GM1, respectively) at different ratios (0-100%), while keeping the total concentration of targets on the surface to 0.01%. The target concentration was kept low to prevent saturation of liposome binding on the surface, and to be able to detect single liposomes. A schematic illustration of the liposome binding to the model surface is shown in figure 21A. The two different liposomes were successfully detected individually using both fluorescence microscopy (Fig. 21B) and ToF-SIMS (Fig. 21C).
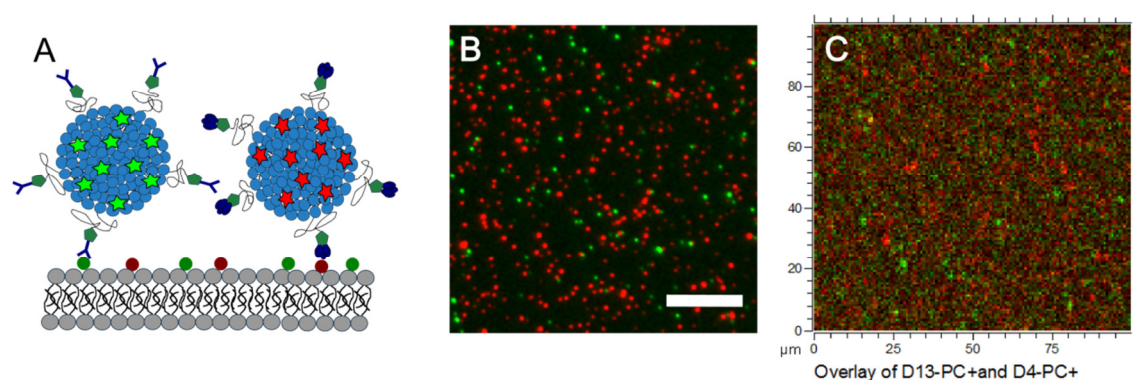

Figure 21 (A) Schematic illustration of the binding of antibiotin- (green) and Chtx- (red) conjugated liposomes to a SLB with biotin and GM1. (B) Fluorescence image (40× magnification) showing the binding of both antibiotin liposomes (labeled with ATTO 488, green) and Chtx liposomes (labeled with Rhodamine, red), for multiplexed detection of biotin and GM1 in a SLB. Scale bar = 25 µm. (C) ToF-SIMS image at high spatial resolution (100×100 µm^2), showing the distribution of antibiotin (detected by the D4-PC+ ions, green) and Chtx (detected by the D13-PC+ ions, red) liposomes, corresponding to biotin and GM1 on the surface.

To be able to quantify the concentration of each liposome on the surface (corresponding to each target), eight different model surfaces with different ratios (0-100%) of each target (biotin or GM1, respectively) were used. The results show an increase in signal intensity with increasing concentration of each target on the surface (Fig. 22) and this trend was evident both with fluorescence microscopy (A) and ToF-SIMS (B). However, the Chtx liposomes (red) produced higher signal intensity, compared to the antibiotin-liposomes (green) at almost all model surfaces. This suggests that the Chtx liposomes bind more efficiently to the surface than the antibiotin liposomes. Although the reason for this difference is not known and needs further investigations, possible explanations include better binding of the Chtx liposomes to GM1 compared to the corresponding antibody binding to biotin, or more efficient exposure of the GM1 target on the surface compared to biotin.

Furthermore, the binding of each type of liposome was quite low in relation to the absolute target concentrations expected from the target mixing ratios in the SLBs. If all targets in the SLB were available for liposome binding, a fully covered liposome layer would be expected to form at target concentrations well below the 0.01% value used in this experiment. However, saturation of the liposome binding did not occur even when the target concentration was raised to 1%. The reason for the relatively low liposome concentrations at high target concentrations is not known and needs to be further investigated.
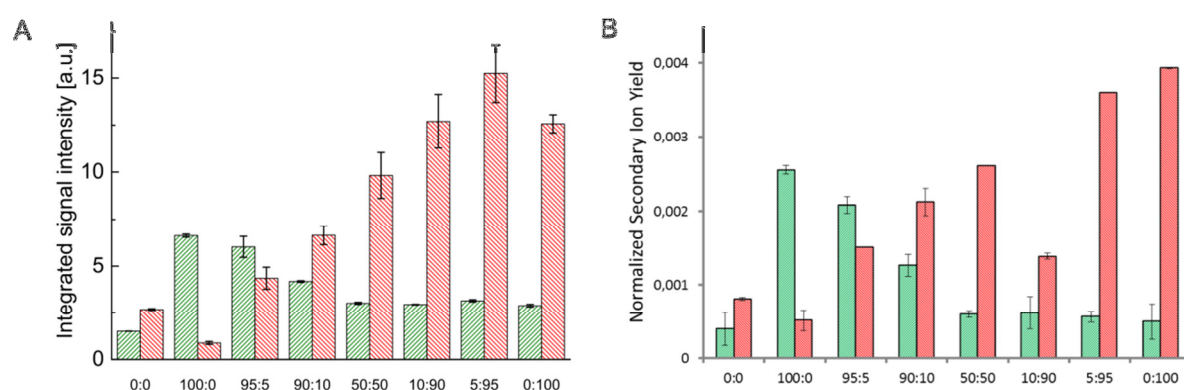

Figure 22 Signal intensities from antibiotin (green) and Chtx liposomes (red) on surfaces containing different ratios (0-100%) biotin:GM1, detected with (A) fluorescence microscopy and (B) ToF-SIMS. The secondary ion yield was normalized to the total ion signal. 0:0 refers to the control surface with only POPC. The standard deviations are based on two samples (n=2).

5. DISCUSSION & OUTLOOK

In this thesis, several approaches for detection of biomolecules on surfaces using IMS have been presented. First of all the liposome approach for detection of specific targets with ToF-SIMS was presented, using the biotinylated liposomes for detection of different concentrations neutravidin on a model surface in paper I, and for detection of Aβ peptides in tissue sections in paper II. The development of protein-conjugated liposomes, for specific detection of multiple targets on the sample surface, was demonstrated for detection of Aβ in tissue sections in paper III, and for multiplexed detection of both biotin and GM1 in a SLB in paper V. The liposome approach presented in this thesis provides a new methodology for detection of proteins on surfaces using ToF-SIMS, since the liposomes are easily detected and distinguished in the mass spectrum using specific deuterated lipids, while the proteins themselves cannot be identified or distinguished due to fragmentation during the ion bombardment. An advantage of using ToF-SIMS for imaging of tissue sections is the parallel detection of several native lipids, without labeling or *a priori* knowledge. Most methods for investigation of lipids cannot provide the spatial distribution of the molecules, but using ToF-SIMS imaging, a spatial resolution of <1 μm can be obtained.

However, several obstacles need to be further investigated and protocols need to be further optimized to minimize nonspecific binding of the liposomes, which was observed in this work on the SLBs, but also in the tissue sections. Also, the binding efficiency between the recognition elements on the liposomes and the targets on the sample surface needs to be investigated for accurate quantification of different targets on the surfaces.

Furthermore, more studies are needed to investigate lipid migration during the preparation of the tissue, especially with focus on cholesterol and sulfatides, to reveal their native distribution in relation to Aβ deposits. Solé-Domenèch et al. discovered small, cholesterol enriched inclusions close to Aβ deposits in AD mouse brains (Solé-Domènech et al. 2013). However, these inclusions have only been observed when analyzing the tissue in a frozen state. Since cholesterol has been shown to migrate to the surface when the temperature is elevated in vacuum, these studies must be done carefully for correct interpretation (Sjövall et al. 2006). Cholesterol accumulation on the surface is not desired, not only because it gives the wrong spatial information, but also because of its ability to suppress the ionization of other lipids in the surrounding tissue (Angerer et al. 2015b).

Using MALDI imaging, Aβ deposits could be detected in tissue sections without any labeling with liposomes, revealing the identity of several Aβ peptides in specific regions of the mouse brain. Further analysis of the mass spectrum revealed several other peptides/proteins associated with the deposits, where one could be putatively identified as the macrophage migration inhibitory factor (MIF), which is an important component in neuroinflammatory processes in the brain. However, due to extensive preparation of the tissue section prior to analysis, lipids cannot be detected at the same time as the proteins with MALDI. Instead, an adjacent tissue section can be analyzed for this purpose, by optimizing the preparation for detection of lipids instead of proteins. Furthermore, the spatial resolution is not as good in MALDI as with ToF-SIMS, thus limiting the field of view from subcellular structures to tissue regions.

Thus, none of the imaging techniques discussed in this thesis provides a complete picture of all the molecules involved in the generation of AD. Instead, they are complementary, and by using several analysis methods on the same, or adjacent tissue sections, more information can be obtained about possible interactions and components in the disease progression.

Moreover, for investigation of the generation of Aβ deposition in the brain, analysis at different stages of the disease is needed, which can be performed using mice sacrificed at different ages (Lord et al. 2006). However, in this way there will also always be individual fluctuations between the different tissue samples. But, using the method described above for MALDI imaging, this could reveal when the Aβ deposition starts to be apparent, and which Aβ peptides or regions that are first involved in the process. Also, other important molecules could be revealed, some may even be age-dependent, which opens up for the discovery of new biomarkers for disease development.

ToF-SIMS imaging with liposomes directed to Aβ at earlier stages of AD might shed more light on the aberrant lipid regulation associated with Aβ deposition, such as cholesterol dysregulation or sulfatide depletion (Han 2010; Puglielli et al. 2003). Also, if the problems with nonspecific binding can be circumvented, detection of intracellular Aβ accumulation might be possible, in combination with the detection of aberrant Tau pathology, by directing other immunoliposomes to hyperphosphorylated Tau fibrils or neurofibrillary tangles. Also, the possibility to detect and image GM1 in the plasma membrane, using the developed Chtx liposomes (paper V), in combination with the liposomes directed to Aβ, offers an interesting approach for determination of the aggregation process of monomeric Aβ peptides into

deposits (Kakio et al. 2001), especially in younger animals at an earlier stage of the disease. Also, clinical samples from patients with AD would be interesting to investigate with ToF-SIMS using the liposomes, for detection of other unknown biomolecules, such as lipids or metabolites, involved in the disease progression.

There are thus many interesting approaches to continue the investigation of biological surfaces with IMS, which could play an important role for revealing complex molecular mechanisms involved in neurodegeneration and for the discovery of new biomarkers associated with AD.

6. CONCLUSIONS

In this thesis, several methods for detection of lipids and proteins on biological surfaces have been investigated. Using ToF-SIMS imaging, in combination with antibody-coupled liposomes, it was possible to image the distribution of Aβ peptides in parallel with several lipids, such as cholesterol and sulfatides, in tissue sections from AD mouse brains. It was also possible to detect two different targets, the vitamin biotin and the glycosphingolipid GM1, respectively, at the same time in a SLB using the liposome approach. This method thus provides new opportunities to investigate interactions between lipids and proteins in biological samples.

Using MALDI imaging, it was possible to investigate the spatial distribution and peptide composition of Aβ deposits in mouse brains. In this way, several different Aβ species were identified, in specific mouse brain regions. Also, other peptide species were discovered to colocalize with Aβ, of which one was identified as the macrophage migration inhibitory factor. This method opens up for the discovery of new biomolecules involved in the generation of AD and may thus give new insights into the disease mechanism as well as providing new potential biomarkers for disease progression.

7. ACKNOWLEDGEMENTS

First of all, I would like to acknowledge my main supervisor, Peter Sjövall, for being supportive and encouraging during my Ph.D. Thank you for being available for valuable discussions and for carefully and thoroughly scrutinizing the work presented in this thesis.

I would also like to acknowledge Prof. Fredrik Höök at the biological physics group, for being supportive and for interesting discussions. Furthermore, I would like to thank all my colleagues in the biological physics group for providing such a friendly and nice working atmosphere. Especially I would like to thank Anders G, Björn A, Hudson, Anders L, Sabina and Nagma for very valuable discussions. Thank you Juliane for the kind gifts at fika-time :) And thanks to Julie for the nice talks, whenever and wherever. Also, thanks to Sanna (at chemistry) for the nice discussions when planning for the soft matter lunch seminars.

To my collaborators at Karolinska Institutet; Martin, Björn, Santi, Vladana and Ida, thank you for all interesting discussions and for making this Alzheimer's project possible. And thank you for welcoming me to your group at any time. Especially thanks to Vladana for helping me with the confocal microscope and for your feedback on the thesis!

Thanks to my MALDI collaborator, Jörg. I really appreciate your help with understanding the technique, and I am glad that it resulted in such a nice paper.

To my manager, Benny, and my colleagues at SP Medtech division; thank you for being supporting whenever needed and thanks for providing a very nice atmosphere in the group. Especially thanks to Kristina for valuable feedback on the thesis. I would also like to thank the members of Gemenskapen, Elva, Camilla L, Haleh, Per, Therese, Marcus, Hanna and Mathias, for the nice and inspiring discussions and for making the work environment even better.

To my family and friends, thank you for being a part of my life and for being continuously supportive. And thanks for trying to understand what I am doing; it means a lot to me!

To my love and fiancé, Sebastian, thank you for your support and for being in my life and making it much more precious. Team cat-lovers ftw! Also I would like to acknowledge my two adorable cats, Zoe and Inka, for bringing me tremendous comfort for the soul. Although maybe not at 5 o'clock in the morning...

And, finally, thanks to you for reading this thesis; I really hope you find it interesting!

REFERENCES

Alberts, Bruce; Johnson, Alexander; Lewis, Julian; Raff, Martin; Roberts, Keith; Walter, Peter (2002), *Molecular biology of the cell* (4:th edn.; New York: Garland Science).

Allen, Theresa M and Cullis, Pieter R (2013), 'Liposomal drug delivery systems: from concept to clinical applications', *Advanced drug delivery reviews,* 65 (1), 36-48.

Angelo, Michael, et al. (2014), 'Multiplexed ion beam imaging of human breast tumors', *Nat Med*.

Angerer, Tina B, Blenkinsopp, Paul, and Fletcher, John S (2015a), 'High energy gas cluster ions for organic and biological analysis by time-of-flight secondary ion mass spectrometry', *International Journal of Mass Spectrometry,* 377, 591-98.

Angerer, Tina B, et al. (2015b), 'Improved Molecular Imaging in Rodent Brain with Time-of-Flight-Secondary Ion Mass Spectrometry Using Gas Cluster Ion Beams and Reactive Vapor Exposure', *Analytical Chemistry,* 87 (8), 4305-13.

Arinaminpathy, Yalini; Khurana, Ekta; Engelman, Donald M; Gerstein, Mark B (2009), 'Computational analysis of membrane proteins: the largest class of drug targets', *Drug Discov Today,* 14 (23-24), 1130-35.

Arriagada, Paulina V, et al. (1992), 'Neurofibrillary tangles but not senile plaques parallel duration and severity of Alzheimer's disease', *Neurology,* 42 (3), 631-31.

Ballard, Clive, et al. (2011), 'Alzheimer's disease', *The Lancet,* 377 (9770), 1019-31.

Ballatore, Carlo, Lee, Virginia M-Y, and Trojanowski, John Q (2007), 'Tau-mediated neurodegeneration in Alzheimer's disease and related disorders', *Nature reviews neuroscience,* 8 (9), 663-72.

Barone, Eugenio, Di Domenico, Fabio, and Butterfield, D Allan (2014), 'Statins more than cholesterol lowering agents in Alzheimer disease: their pleiotropic functions as potential therapeutic targets', *Biochemical pharmacology,* 88 (4), 605-16.

Belazi, D., et al. (2009), 'Chemical analysis of osmium tetraoxide staining in adipose tissue using imaging ToF-SIMS', *Histochem. Cell. Biol.,* 132, 105-15.

Benabdellah, F., et al. (2010), 'Mass spectrometriy imaging of rat brain sections: nanomolar sensitivity with MALDI versus nanometer resolution by TOF-SIMS', *Anal. Bioanal. Chem.,* 396, 151-62.

Benninghoven, A (1973), 'Surface investigation of solids by the statical method of secondary ion mass spectroscopy (SIMS)', *Surface Science,* 35, 427-57.

Berlier, Judith E, et al. (2003), 'Quantitative comparison of long-wavelength Alexa Fluor dyes to Cy dyes: fluorescence of the dyes and their bioconjugates', *Journal of Histochemistry & Cytochemistry,* 51 (12), 1699-712.

Berrueta Razo, Irma, et al. (2014), 'Comparing C60+ and (H2O) n+ clusters for mouse brain tissue analysis', *Surface and Interface Analysis,* 46 (S1), 136-39.

Bich, C., et al. (2013a), 'Compatibility between TOF-SIMS lipid imaging and histological staining on a rat brain section', *Surf. Interface Anal.,* 45 (1), 260-63.

Bich, Claudia, Touboul, David, and Brunelle, Alain (2015), 'Biomedical studies by TOF-SIMS imaging', *Biointerphases,* 10 (1), 018901.

Bich, Claudia, et al. (2013b), 'Argon Cluster Ion Source Evaluation on Lipid Standards and Rat Brain Tissue Samples', *Anal. Chem.,* 85 (16), 7745-52.

Bingen, Pit, et al. (2008), 'Solvation Effects in the Quartz Crystal Microbalance with Dissipation Monitoring Response to Biomolecular Adsorption. A Phenomenological Approach', *Analytical Chemistry,* 80 (23), 8880-90.

Boxer, Steven G., Kraft, Mary L., and Weber, Peter K. (2009), 'Advances in Imaging Secondary Ion Mass Spectrometry for Biological Samples', *Annual Review of Biophysics,* 38 (1), 53-74.

Breitenstein, D., et al. (2007), 'The chemical composition of animal cells and their intracellular compartments reconstructed from 3D mass spectrometry', *Angew Chem Int Ed Engl,* 46 (28), 5332-5.

Brunelle, A., Touboul, D., and Laprévote, O. (2005), 'Biological tissue imaging with time-of-flight secondary ion mass spectrometry and cluster ion sources', *Journal of Mass Spectrometry,* 40 (8), 985-99.

Brunelle, Alain and Laprévote, Olivier (2009), 'Lipid imaging with cluster time-of-flight secondary ion mass spectrometry', *Analytical and Bioanalytical Chemistry,* 393 (1), 31-35.

Caprioli, Richard M., Farmer, Terry B., and Gile, Jocelyn (1997), 'Molecular Imaging of Biological Samples: Localization of Peptides and Proteins Using MALDI-TOF MS', *Analytical Chemistry,* 69 (23), 4751-60.

Carlred, Louise, et al. (2016a), 'Imaging of amyloid-β in Alzheimer's disease transgenic mouse brains with ToF-SIMS using immunoliposomes', *Biointerphases,* 11 (2), 02A312.

Carlred, Louise, et al. (2016b), 'Probing Amyloid-β Pathology in transgenic Alzheimer's disease (tgArcSwe) mice using MALDI Imaging Mass Spectrometry', *Journal of Neurochemistry*, n/a-n/a.

Carlred, Louise, et al. (2014), 'Simultaneous Imaging of Amyloid-β and Lipids in Brain Tissue using Antibody-Coupled Liposomes and Time-of-Flight Secondary Ion Mass Spectrometry', *Journal of the American Chemical Society,* 136 (28), 9973-81.

Cerruti, Christopher D., et al. (2012), 'MALDI Imaging and Structural Analysis of Rat Brain Lipid Negative Ions with 9-Aminoacridine Matrix', *Analytical Chemistry,* 84 (5), 2164-71.

Chait, B. T. and Standing, K. G. (1981), 'A time-of-flight mass spectrometer for measurement of secondary ion mass spectra', *International Journal of Mass Spectrometry and Ion Physics,* 40 (2), 185-93.

Chalfie, Martin, et al. (1994), 'Green fluorescent protein as a marker for gene expression', *Science,* 263 (5148), 802-05.

Chaurand, Pierre, et al. (2004), 'Integrating histology and imaging mass spectrometry', *Analytical Chemistry,* 76 (4), 1145-55.

Chughtai, Kamila and Heeren, Ron M. A. (2010), 'Mass Spectrometric Imaging for biomedical tissue analysis', *Chemical reviews,* 110 (5), 3237-77.

Cipriani, Gabriele, et al. (2011), 'Alzheimer and his disease: a brief history', *Neurological Sciences,* 32 (2), 275-79.

Citron, Martin, et al. (1992), 'Mutation of the β-amyloid precursor protein in familial Alzheimer's disease increases β-protein production', *Nature,* 360 (6405), 672-74.

Cornett, Dale S, et al. (2007), 'MALDI imaging mass spectrometry: molecular snapshots of biochemical systems', *Nature methods,* 4 (10), 828-33.

Deutskens, Fabian, Yang, Junhai, and Caprioli, Richard M (2011), 'High spatial resolution imaging mass spectrometry and classical histology on a single tissue section', *Journal of Mass Spectrometry,* 46 (6), 568-71.

Di Paolo, G. and Kim, T. W. (2011), 'Linking lipids to Alzheimer's disease: cholesterol and beyond', *Nat Rev Neurosci,* 12 (5), 284-96.

Ehehalt, R. (2003), 'Amyloidogenic processing of the Alzheimer beta-amyloid precursor protein depends on lipid rafts', *J. Cell Biol.,* 160 (1), 113-23.

Fletcher, John S, et al. (2007), 'TOF-SIMS 3D biomolecular imaging of Xenopus laevis oocytes using buckminsterfullerene (C60) primary ions', *Analytical Chemistry,* 79 (6), 2199-206.

Frisz, Jessica F., et al. (2013), 'Direct chemical evidence for sphingolipid domains in the plasma membranes of fibroblasts', *Proceedings of the National Academy of Sciences,* 110 (8), E613–E22.

Frost, Rickard, et al. (2013), 'Acoustic detection of melanosome transport in Xenopus laevis melanophores', *Analytical Biochemistry,* 435 (1), 10-18.

Gilmore, IS and Seah, MP (2002), 'Electron flood gun damage in the analysis of polymers and organics in time-of-flight SIMS', *Applied Surface Science,* 187 (1), 89-100.

Gouras, Gunnar K, Willén, Katarina, and Faideau, Mathilde (2013), 'The inside-out amyloid hypothesis and synapse pathology in Alzheimer's disease', *Neurodegenerative Diseases,* 13 (2-3), 142-46.

Gouras, Gunnar K, Olsson, Tomas T, and Hansson, Oskar (2015), 'β-amyloid Peptides and Amyloid Plaques in Alzheimer's Disease', *Neurotherapeutics,* 12 (1), 3-11.

Guerquin-Kern, J, et al. (2005), 'Progress in analytical imaging of the cell by dynamic secondary ion mass spectrometry (SIMS microscopy)', *Biochim. Biophys. Acta,* 1724 (3), 228-38.

Gunnarsson, A., Sjövall, P., and Höök, F. (2010a), 'Liposome-Based Chemical Barcodes for Single Molecule DNA Detection Using Imaging Mass Spectrometry', *Nano Lett.,* 10 (2), 732-37.

Gunnarsson, A., et al. (2008), 'Single-molecule detection and mismatch discrimination of unlabeled DNA targets', *Nano Lett,* 8 (1), 183-8.

Gunnarsson, A., et al. (2010b), 'Spatial-resolution limits in mass spectrometry imaging of supported lipid bilayers and individual lipid vesicles', *Analytical Chemistry,* 82, 2426.

Han, X. L. (2010), 'Multi-dimensional mass spectrometry-based shotgun lipidomics and the altered lipids at the mild cognitive impairment stage of Alzheimer's disease', *Biochim. Biophys. Acta, Mol. Cell Biol. Lipids,* 1801 (8), 774-83.

Hanrieder, Jörg, et al. (2011), 'MALDI mass spectrometry based molecular phenotyping of CNS glial cells for prediction in mammalian brain tissue', *Analytical and Bioanalytical Chemistry,* 401 (1), 135-47.

Henss, Anja, et al. (2016), 'Time of flight secondary ion mass spectrometry of bone—Impact of sample preparation and measurement conditions', *Biointerphases,* 11 (2), 02A302.

Huwyler, Jörg, Wu, Dafang, and Pardridge, William M. (1996), 'Brain drug delivery of small molecules using immunoliposomes', *Proceedings of the National Academy of Sciences,* 93 (24), 14164-69.

Höök, F., et al. (1998), 'Energy Dissipation Kinetics for Protein and Antibody−Antigen Adsorption under Shear Oscillation on a Quartz Crystal Microbalance', *Langmuir,* 14 (4), 729-34.

Höök, F., et al. (2001), 'Variations in Coupled Water, Viscoelastic Properties, and Film Thickness of a Mefp-1 Protein Film during Adsorption and Cross-Linking: A Quartz Crystal Microbalance with Dissipation Monitoring, Ellipsometry, and Surface Plasmon Resonance Study', *Analytical Chemistry,* 73 (24), 5796-804.

Jensen, Ellen (2014), 'Technical review: Colocalization of antibodies using confocal microscopy', *The Anatomical Record,* 297 (2), 183-87.

Jones, Emrys A., Lockyer, Nicholas P., and Vickerman, John C. (2007), 'Mass spectral analysis and imaging of tissue by ToF-SIMS—The role of buckminsterfullerene, C60+, primary ions', *International Journal of Mass Spectrometry,* 260 (2–3), 146-57.

--- (2008), 'Depth Profiling Brain Tissue Sections with a 40 keV C60+ Primary Ion Beam', *Anal. Chem.,* 80 (6), 2125-32.

Jousma, H., et al. (1987), 'Characterization of liposomes. The influence of extrusion of multilamellar vesicles through polycarbonate membranes on particle size, particle size distribution and number of bilayers', *International Journal of Pharmaceutics,* 35 (3), 263-74.

Jølck, Rasmus I, et al. (2010), 'Engineering liposomes and nanoparticles for biological targeting', *Biofunctionalization of Polymers and their Applications* (Springer), 251-80.

Kakio, Atsuko, et al. (2001), 'Cholesterol-dependent formation of GM1 ganglioside-bound amyloid β-protein, an endogenous seed for Alzheimer amyloid', *Journal of Biological Chemistry,* 276 (27), 24985-90.

Keller, C. A. and Kasemo, B. (1998), 'Surface specific kinetics of lipid vesicle adsorption measured with a quartz crystal microbalance', *Biophys J,* 75 (3), 1397-402.

Kim, Jungsu, Basak, Jacob M, and Holtzman, David M (2009), 'The role of apolipoprotein E in Alzheimer's disease', *Neuron,* 63 (3), 287-303.

LaFerla, Frank M (2002), 'Calcium dyshomeostasis and intracellular signalling in Alzheimer's disease', *Nature reviews neuroscience,* 3 (11), 862-72.

Lakowicz, Joseph R. (2006), 'Principles of Fluorescence Spectroscopy', (3:rd ed. edn.; Baltimore, USA: Springer Science+Business Media, LLC), 15.

Lazar, A., et al. (2013), 'Time-of-flight secondary ion mass spectrometry (TOF-SIMS) imaging reveals cholesterol overload in the cerebral cortex of Alzheimer's disease patients', *Acta Neuropathol.,* 125, 133-44.

Lichtman, Jeff W. and Conchello, Jose-Angel (2005), 'Fluorescence microscopy', *Nat Meth,* 2 (12), 910-19.

Lippincott-Schwartz, Jennifer and Phair, Robert D (2010), 'Lipids and cholesterol as regulators of traffic in the endomembrane system', *Annual Review of Biophysics,* 39, 559.

Lord, Anna, et al. (2006), 'The Arctic Alzheimer mutation facilitates early intraneuronal Aβ aggregation and senile plaque formation in transgenic mice', *Neurobiology of Aging,* 27 (1), 67-77.

M. Prince, A. Wimo, M. Guerchet, G-C. Ali, Y. Wu, M. Prina, (2015), 'World Alzheimer Report 2015: The Global Impact of Dementia - An analysis of prevalence, incidence, cost and trends', (http://www.alz.co.uk/research/world-report-2015: Alzheimer's Disease International).

Malm, J., et al. (2009), 'Fixation and Drying Protocols for the Preparation of Cell Samples for Time-of-Flight Secondary Ion Mass Spectrometry Analysis', *Anal. Chem.,* 81 (17), 7197-205.

Martin-Lorenzo, Marta, et al. (2014), '30 μm spatial resolution protein MALDI MSI: In-depth comparison of five sample preparation protocols applied to human healthy and atherosclerotic arteries', *Journal of Proteomics,* 108 (0), 465-68.

Mas, Sebastian, et al. (2008), 'Cluster TOF-SIMS imaging: A new light for in situ metabolomics?', *Proteomics,* 8 (18), 3735-45.

Merritt, Ethan A, et al. (1994), 'Crystal structure of cholera toxin B-pentamer bound to receptor GM1 pentasaccharide', *Protein Science,* 3 (2), 166-75.

Monroe, Eric B, et al. (2005), 'Vitamin E imaging and localization in the neuronal membrane', *Journal of the American Chemical Society,* 127 (35), 12152-53.

Nilebäck, Erik, et al. (2011), 'Characterization and application of a surface modification designed for QCM-D studies of biotinylated biomolecules', *Biosensors and Bioelectronics,* 28 (1), 407-13.

Nobs, Leila, et al. (2004), 'Current methods for attaching targeting ligands to liposomes and nanoparticles', *Journal of Pharmaceutical Sciences,* 93 (8), 1980-92.

Nygren, H., et al. (2005), 'Localization of cholesterol, phosphocholine and galactosylceramide in rat cerebellar cortex with imaging TOF-SIMS equipped with a bismuth cluster ion source', *Biochim. Biophys. Acta,* 1737 (2-3), 102-10.

O'Hurley, Gillian, et al. (2014), 'Garbage in, garbage out: a critical evaluation of strategies used for validation of immunohistochemical biomarkers', *Molecular oncology,* 8 (4), 783-98.

Ostrowski, Sara G., et al. (2004), 'Mass Spectrometric Imaging of Highly Curved Membranes During Tetrahymena Mating', *Science,* 305 (5680), 71-73.

Park, J W, et al. (1995), 'Development of anti-p185HER2 immunoliposomes for cancer therapy', *Proceedings of the National Academy of Sciences,* 92 (5), 1327-31.

Passarelli, Melissa K. and Winograd, Nicholas (2011), 'Lipid imaging with time-of-flight secondary ion mass spectrometry (ToF-SIMS)', *Biochimica et Biophysica Acta (BBA) - Molecular and Cell Biology of Lipids,* 1811 (11), 976-90.

Patil, Yogita P and Jadhav, Sameer (2014), 'Novel methods for liposome preparation', *Chemistry and Physics of Lipids,* 177, 8-18.

Pol, J., et al. (2010), 'Molecular mass spectrometry imaging in biomedical and life science research', *Histochem. Cell Biol.,* 134 (5), 423-43.

Pralle, A, et al. (2000), 'Sphingolipid–cholesterol rafts diffuse as small entities in the plasma membrane of mammalian cells', *The Journal of cell biology,* 148 (5), 997-1008.

Puglielli, L., Tanzi, R. E., and Kovacs, D. M. (2003), 'Alzheimer's disease: the cholesterol connection', *Nat Neurosci,* 6 (4), 345-51.

Rahman, SM Jamshedur, et al. (2011), 'Lung cancer diagnosis from proteomic analysis of preinvasive lesions', *Cancer research,* 71 (8), 3009-17.

Razo, Irma Berrueta, et al. (2015), 'Mass spectrometric imaging of brain tissue by time-of-flight secondary ion mass spectrometry–How do polyatomic primary beams C60, Ar2000, water-doped Ar2000 and (H2O) 6000 compare?', *Rapid Commun. Mass Spectrom,* 29, 1851-62.

Reimhult, Erik, Hook, Fredrik, and Kasemo, Bengt (2002), 'Vesicle adsorption on SiO2 and TiO2: Dependence on vesicle size', *Journal of chemical physics,* 117 (16), 7401-04.

Robinson, Michael and Castner, David (2013), 'Characterization of sample preparation methods of NIH/3T3 fibroblasts for ToF-SIMS analysis', *Biointerphases,* 8 (1), 15.

Rodahl, Michael, et al. (1995), 'Quartz crystal microbalance setup for frequency and Q-factor measurements in gaseous and liquid environments', *Review of Scientific Instruments,* 66 (7), 3924-30.

Rohner, T. C., Staab, D., and Stoeckli, M. (2005), 'MALDI mass spectrometric imaging of biological tissue sections', *Mech. Ageing Dev.,* 126 (1), 177-85.

Römpp, Andreas and Spengler, Bernhard (2013), 'Mass spectrometry imaging with high resolution in mass and space', *Histochem. Cell Biol.,* 139 (6), 759-83.

Sauerbrey, G. (1959), 'The use of quartz oscillors for weighing thin layers and microweighing', *Z. Phys.,* 155, 209-22.

Schwartz, Sarah A., Reyzer, Michelle L., and Caprioli, Richard M. (2003), 'Direct tissue analysis using matrix-assisted laser desorption/ionization mass spectrometry: practical aspects of sample preparation', *Journal of Mass Spectrometry,* 38 (7), 699-708.

Schöll, Michael, et al. (2016), 'PET Imaging of Tau Deposition in the Aging Human Brain', *Neuron,* 89 (5), 971-82.

Selkoe, Dennis J. (2008), 'Soluble oligomers of the amyloid β-protein impair synaptic plasticity and behavior', *Behavioural Brain Research,* 192 (1), 106-13.

Severs, Nicholas J; Shotton, David M (2006), 'Rapid freezing of Biological specimens for freeze fracture and deep etching', in Julio E. Celis (ed.), *Cell Biology: A Laboratory Handbook* (3:rd ed. edn.), 249-55.

Shard, Alexander G, et al. (2012), 'Argon cluster ion beams for organic depth profiling: results from a VAMAS interlaboratory study', *Analytical Chemistry,* 84 (18), 7865-73.

Sheets, Erin D, Holowka, David, and Baird, Barbara (1999), 'Membrane organization in immunoglobulin E receptor signaling', *Current Opinion in Chemical Biology,* 3 (1), 95-99.

Shimomura, Osamu, Johnson, Frank H, and Saiga, Yo (1962), 'Extraction, purification and properties of aequorin, a bioluminescent protein from the luminous hydromedusan, Aequorea', *Journal of cellular and comparative physiology,* 59 (3), 223-39.

Siegel, George J. and Ebrary (2006), *Basic neurochemistry: molecular, cellular, and medical aspects* (7th;7;; Burlington, MA: Elsevier Academic).

Simons, Kai and Toomre, Derek (2000), 'Lipid rafts and signal transduction', *Nat Rev Mol Cell Biol,* 1 (1), 31-39.

Sjövall, Peter, et al. (2014), 'Imaging of distribution of topically applied drug molecules in mouse skin by combination of time-of-flight secondary ion mass spectrometry and scanning electron microscopy', *Analytical Chemistry,* 86 (7), 3443-52.

Sjövall, P., Lausmaa, J., and Johansson, B. (2004), 'Mass Spectrometric Imaging of Lipids in Brain Tissue', *Anal. Chem.,* 76, 4271.

Sjövall, P., Johansson, B., and Lausmaa, J. (2006), 'Localization of lipids in freeze-dried mouse brain sections by imaging TOF-SIMS', *Appl. Surf. Sci.,* 252 (19), 6966-74.

Sjövall, P., et al. (2014), 'Liposome binding for multiplexed biomolecule detection and imaging using ToF-SIMS', *Surface and Interface Analysis,* 46 (10-11), 707-11.

Smith, Carolyn L (2008), 'Basic confocal microscopy', *Current Protocols in Molecular Biology*, 14.11. 1-14.11. 18.

Solé-Domènech, S., et al. (2013), 'Localization of cholesterol, amyloid and glia in Alzheimer's disease transgenic mouse brain tissue using time-of-flight secondary ion mass spectrometry (ToF-SIMS) and immunofluorescence imaging', *Acta Neuropathol.,* 125, 145-57.

Speight, Robert E. and Cooper, Matthew A. (2012), 'A Survey of the 2010 Quartz Crystal Microbalance Literature', *Journal of Molecular Recognition,* 25 (9), 451-73.

St George-Hyslop, P. H. (2000), 'Piecing together Alzheimer's', *Sci Am,* 283 (6), 76-83.

Steinhauser, Matthew L and Lechene, Claude P (2013), 'Quantitative imaging of subcellular metabolism with stable isotopes and multi-isotope imaging mass spectrometry', *Seminars in cell & developmental biology* (24: Elsevier), 661-67.

Steinhauser, Matthew L, et al. (2012), 'Multi-isotope imaging mass spectrometry quantifies stem cell division and metabolism', *Nature,* 481 (7382), 516-19.

Stoeckli, Markus, Staab, Dieter, and Schweitzer, Alain (2007), 'Compound and metabolite distribution measured by MALDI mass spectrometric imaging in whole-body tissue sections', *International Journal of Mass Spectrometry,* 260 (2), 195-202.

Swedlow, Jason R (2012), 'Innovation in biological microscopy: current status and future directions', *Bioessays,* 34 (5), 333-40.

Tahallah, N., et al. (2008), 'Lipid mapping in human dystrophic muscle by cluster-time-of-flight secondary ion mass spectrometry imaging', *J. Lipid Res.,* 49 (2), 438-54.

Terry, Robert D, et al. (1991), 'Physical basis of cognitive alterations in Alzheimer's disease: synapse loss is the major correlate of cognitive impairment', *Annals of neurology,* 30 (4), 572-80.

Thakker, Deepak R, et al. (2009), 'Intracerebroventricular amyloid-β antibodies reduce cerebral amyloid angiopathy and associated micro-hemorrhages in aged Tg2576 mice', *Proceedings of the National Academy of Sciences,* 106 (11), 4501-06.

Thambisetty, Madhav and Lovestone, Simon (2010), 'Blood-based biomarkers of Alzheimer's disease: challenging but feasible', *Biomarkers in medicine,* 4 (1), 65-79.

ThermoFisherScientific 'Fluorescence SpectraViewer', <https://www.thermofisher.com/se/en/home/life-science/cell-analysis/labeling-chemistry/fluorescence-spectraviewer.html>.

Thiel, Volker and Sjovall, Peter (2015), 'CHAPTER 5 Time-of-Flight Secondary Ion Mass Spectrometry (TOF-SIMS): Principles and Practice in the Biogeosciences', *Principles and Practice of Analytical Techniques in Geosciences* (The Royal Society of Chemistry), 122-70.

Touboul, D., Laprevote, O., and Brunelle, A. (2011), 'Micrometric molecular histology of lipids by mass spectrometry imaging', *Curr Opin Chem Biol,* 15 (5), 725-32.

Touboul, D., et al. (2004), 'Tissue molecular ion imaging by gold cluster ion bombardment', *Anal. Chem.,* 76 (6), 1550-9.

Tsurui, Hiromichi, et al. (2000), 'Seven-color fluorescence imaging of tissue samples based on Fourier spectroscopy and singular value decomposition', *Journal of Histochemistry & Cytochemistry,* 48 (5), 653-62.

Tymchenko, Nina, et al. (2013), 'Acoustical sensing of cardiomyocyte cluster beating', *Biochemical and Biophysical Research Communications,* 435 (4), 520-25.

Walsh, Dominic M. and Selkoe, Dennis J. (2007), 'A? Oligomers ? a decade of discovery', *Journal of Neurochemistry,* 101 (5), 1172-84.

Wenk, M. R. (2005), 'The emerging field of lipidomics', *Nature Rev. Drug Discovery,* 4 (7), 594-610.

Vickerman, J.C. and Briggs, D. (eds.) (2001), *ToF-SIMS - Surface analysis by mass spectrometer* (Chichester, Manchester: IM Publications and SurfaceSPectra Limited).

Wilson, R. L., et al. (2012), 'Fluorinated colloidal gold immunolabels for imaging select proteins in parallel with lipids using high-resolution secondary ion mass spectrometry', *Bioconjugate Chem.,* 23, 450-60.

Voinova, M. V., et al. (1999), 'Viscoelastic Acoustic Response of Layered Polymer Films at Fluid-Solid Interfaces: Continuum Mechanics Approach', *Physica Scripta,* 59 (5), 391.

Yamada, Hideaki, et al. (2010), 'MeV-energy probe SIMS imaging of major components in animal cells etched using large gas cluster ions', *Nuclear Instruments and Methods in Physics Research Section B: Beam Interactions with Materials and Atoms,* 268 (11), 1736-40.

Yanagisawa, Katsuhiko (2007), 'Role of gangliosides in Alzheimer's disease', *Biochimica et Biophysica Acta (BBA)-Biomembranes,* 1768 (8), 1943-51.

Yeager, Ashley N, Weber, Peter K, and Kraft, Mary L (2016), 'Three-dimensional imaging of cholesterol and sphingolipids within a Madin-Darby canine kidney cell', *Biointerphases,* 11 (2), 02A309.

Zetterberg, Henrik, et al. (2010), 'Biochemical markers in Alzheimer's disease clinical trials', *Biomarkers in medicine,* 4 (1), 91-98.

Zhang, Duan-Sun, et al. (2012), 'Multi-isotope imaging mass spectrometry reveals slow protein turnover in hair-cell stereocilia', *Nature,* 481 (7382), 520-24.